Hydro-climatology study of the Ogooué River basin using hydrological modeling and satellite altimetry

Sakaros Bogning, Frédéric Frappart, Adrien Paris, Fabien Blarel, Fernando Niño, Stéphane Saux Picart, Pauline Lanet, F. Seyler, Gil Mahé, Raphael Onguene, et al.

Version of Record: https://www.sciencedirect.com/science/article/pii/S0273117720302180
Manuscript_da7fe5fe1ad76a5da2f90248055d8d2d

Hydro-climatology study of the Ogooué River basin using hydrological modeling and satellite altimetry

Sakaros Bogning[a,b,g,j*], Frederic Frappart[b,*], Adrien Paris[c], Fabien Blarel[b], Fernando Niño[b], Stéphane Saux Picart[d], Pauline Lanet[d], Frederique Seyler[e], Gil Mahé[f], Raphael Onguene[g], Jean-Pierre Bricquet[f], Jacques Etame[a], Marie-Claire Paiz[h] and Jean-Jacques Braun[j]

[a]*University of Douala, Department of Earth Sciences, Douala, Cameroon.*

[b]*LEGOS Université de Toulouse, CNES, CNRS, IRD, UPS OMP, 14 Av. E. Belin, 31400 Toulouse, France.*

[c]*Collecte Localisation Satellite (CLS), Ramonville-Saint-Agne, 31520, France*

[d]*CNRM, Université de Toulouse, Météo-France, CNRS, Lannion, France.*

[e]*ESPACE-DEV, Université de Montpellier, IRD, Université des Antilles, Université de Guyane, Université de La Réunion, Maison de la Télédétection, 500 Rue J-F. Breton, 34093 Montpellier, France*

[f]*HydroSciences Montpellier, Université de Montpellier–CC 57, 163 rue Auguste Broussonnet, 34090 Montpellier, France*

[g]*University of Douala, JEAI-RELIFOME, Douala, Cameroon.*

[h]*The Nature Conservancy, 114 rue Bana Ba Kengue, Haut de Gué Gué, Libreville, Gabon.*

[J]*LMI DYCOFAC, Institut de Recherche pour le Développement, BP 1857 Yaoundé, Cameroon.*

[*] *Corresponding author: sakaros.bogning@legos.obs-mip.fr*

Abstract

Hydrological models are important tools for the simulation of water storage and hydrological fluxes in large basins and complex river systems. The hydrological models can compensate the lack of observed data in ungauged basins. In this study, the hydrological model of large basins MGB (for Model of Large Basins in Portuguese) is used to evaluate the hydrological processes of the Ogooué River Basin (ORB), which has been mostly unmonitored for about three decades. Simulations were carried out over an 18-year period from 1998 to 2015 using TRMM 3B42 daily rainfall data from the Tropical Rainfall Measurement Mission (TRMM) as forcing and in situ and altimetry-based river discharges from Envisat, Saral Altika and Jason-2 for calibration and validation. The results of the model were in good agreement with the flows measured at stations upstream and downstream of the Ogooué basin (Nash-Sutcliffe Efficiency (NSE)> 0.56 for all calibration gauges). The MGB model efficiently describes the seasonal and interannual variations of the flow in the Ogooué River and its major tributaries which were found to be highly correlated to the rainfall (r ranging from 0.72 to 0.90 and 0.56 to 0.87 at seasonal and interannual time-scales respectively). Interannual variations of precipitation and river discharge of the ORB are linked to the El Niño Southern Oscillation (ENSO) in the tropical eastern Pacific Ocean and southeastern tropical Atlantic Niño. Also, the Ogooué river discharge was found to be strongly correlated with Sea Surface Temperature (SST) at annual and semi-annual time-scales.

Keywords: *altimetry; ENSO; MGB model; rainfall variability, river discharge; tropical Atlantic Niño.*

1. Introduction

The interannual variations of rainfall and flow are most likely related to climatic phenomena. Numerous authors have investigated factors affecting rainfall variability in western equatorial Africa without reaching any concrete consensus as these factors vary strongly, both spatially and temporally (Nicholson 2018). The most commonly evoked mechanism to explain past and present changes in tropical African rainfall is a shift in the mean annual position of the Intertropical Convergence Zone (ITCZ), which migrates meridionally, and is potentially driven by seasonally and orbitally driven changes in interhemispheric heat distribution (Haug et al. 2001; Tierney et al. 2008; Kodja 2018). Recently, Djoufack (2011) explained the mechanism as follows: the distribution of the centers of action corresponds to a surface circulation, characterized by east-easterly winds originating from the north-east (Harmattan) in the northern hemisphere and the south-west in the southern hemisphere (trade winds), which give rise to ITCZ near the equator. The meridian circulation advects monsoon air from the Gulf of Guinea while drier air is simultaneously advected by the Saharan depressions. The contact of these two air masses with different thermodynamic properties in the lower layers (near the intertropical front) creates meridian gradients and sets up sources of instability that interact with convective mesoscale systems and precipitating systems (Nnamchi et al. 2015). The concept of ITCZ has been generally associated with maximum rainfall and used to explain the bimodal regime of rainfall in the equatorial zone with the twice-equatorial transit of the ITCZ and the unimodal regime in the outer tropical regions corresponding to the extreme latitudinal positions of the ITCZ (Djoufack 2011; Kodja 2018). It has been delineated by the more or less discontinued line of clouds visible as white spots on satellite images –cold top clouds, which helped Citeau et al. (1988) to represent its seasonal and inter-annual variability between 1970 and 1987. Nicholson (2018) recently

pointed out the extensive use of ITCZ in other scientific disciplines like geology, ecology, paleoclimatology, and history.

However, Nicholson (2018) also summarized the many controversies related to the ITCZ concept. Its definitions depend on the geophysical parameters used and hence can lead to some ambiguities. Besides, the heterogeneity of rainfall patterns of the tropical African zone cannot be disregarded: if the ITCZ and maximum rainfall shift latitudinally with seasons, we also have to take into account that they fluctuate independently from year to year in the north of the Gulf of Guinea (Grist and Nicholson 2001). Moreover, such rainfall patterns have never been described for equatorial Africa (Nicholson 2018). Although rainfall dynamic over west equatorial Africa is mainly affected by the West African monsoon, the ITCZ being widely used to explain rainfall variations in West Africa seems inappropriate for understanding rainfall fluctuations and therefore the evolution of the hydrological cycle in the poorly gauged river basins of Central Equatorial Africa.

The Ogooué River Basin (ORB) is an equatorial coastal area of central Africa spanning about 80 % of the total area of Gabon (Braun et al. 2015). Almost half of the Gabonese population directly depend on water resources from the Ogooué River and its tributaries for freshwater supply, electricity production, transport, sand extraction, and agriculture on both individual to industrial scales (D.G.S. 2015). However, this harmoniously kept pace, long maintained between the population and the environment, could be brought to an end as anthropogenic activities such as deforestation, adding up to global climate change threats. Deforestation was happening in the ORB at a rate of 0.38% from 1990 to 2000 and almost the same loss rate since 2000 (Fichet et al. 2014). Furthermore, Gabon recently launched an ambitious development plan, with transportation infrastructure, agriculture, forestry, and mining projects which increase the pressure on water resources and could negatively affect available water quantities, despite the willingness of the authorities to make the country emergent

based on an ambitious ecological program (Gambotti 2014). Even though Gabonese authorities are looking for information to allow a precise understanding of the current changes occurring in the basin in order to make appropriate decisions that will preserve the biodiversity of this fragile and threatened environment (Gambotti 2014), the in situ environmental monitoring systems were not maintained after the mid-80s for the latest observations (Mahé et al. 1990).

Recently, several studies demonstrated the potential of satellite observations of surface water levels, sometimes in combination with hydrological modeling, to estimate freshwater discharges (Bogning et al. 2018; Kittel et al. 2018). Their results might be useful for addressing integrated water resources management policies in the ORB. But, as they are based on the use of radar altimetry-based water levels, their use remains limited because of the current drawbacks of this type of remotely sensed observations for hydrological studies. In spite of the improvement of acquisition techniques which include closed-loop acquisition mode based on the use of a digital elevation model – DEM – allowing to retrieve reliable water levels in valley bottoms (Biancamaria et al. 2018) and synthetic aperture radar – SAR – technique providing accurate water levels even over small rivers (Bogning et al. 2018; Normandin et al. 2018), the repeat period of the current altimetry missions (longer than 10 days) is not sufficient enough to monitor rapid changes in the water levels (Biancamaria et al. 2017). Combined with in situ data through hydrological modeling – remote sensing coupled approaches, they are starting to be used to analyze the temporal variations of river discharge in large river basins such as the Amazon (Paris et al. 2016), the Niger (Fleischmann et al. 2018), and the Ganga-Brahmaputra river basin (Maswood and Hossain 2016). But,this approach was not frequently used in a quasi-ungauged river basin of smaller size.

In this study, the hydrological model of large basins (MGB) (Collischonn et al. 2007) is used to simulate the spatio-temporal variations in river discharges in the almost ungauged Ogooué

River Basin located in Gabon (Central Africa). Simulations were carried out from 2001 to 2015 using daily rainfall estimates from the Tropical Rainfall Measurement Mission (TRMM) as forcing, and both in-situ and altimetry derived water stages and discharges for calibration and validation. The simulated variations of river discharges in the ORB were related to changes in rainfall in response to climate variability. Their impact on the sea surface temperature at the Ogooué mouth was also analyzed.

2. The Ogooué River Basin

The ORB is located in central Africa, between 9° and 15°E, and 3°S and 2.5°N. Its drainage area is about 220,000 km^2, covering most of Gabon and small areas in Cameroon and Congo (Figure 1). The three main types of terrain encountered in the ORB are plains, plateaus, and mountains. Low and flat plains (with altitudes no higher than 300 m) are found downstream of the ORB, from the delta of Ogooué to Lopé, covering the lake region in the interior delta of Ogooué, along the Ogooué River and the Ngounié basin. Plateaus are sometimes heavily cut by rivers and cover most of the area of the ORB: they extend north of the Ivindo river basin, southeast upstream of the Ogooué River and to the south on the Ngounié river basin. These plateaus range from 300 to 800 m. Towards the interior of the ORB, south of the Ogooué River, some medium mountain ranges form true chains; this is the case of the northern mountains of the Mayombé range and the Chaillu massif with some peaks reaching 1000 m.

The ORB is located in the equatorial climate zone near the Atlantic Ocean. The rainfall regime in the ORB is bimodal like those of most equatorial river basins. According to Mahé et al. (1990), the long equatorial dry season lasts about two months (July-August) in the northern part of the basin and increases gradually towards the south to nearly four months (June to September). From September to January, the monsoon winds penetrate Gabon from

the north, reaching the south in October, causing abundant rainfall known as the great rainy season. In the north of Gabon, higher precipitations are recorded in October (ranging from 250 to over 600 mm), and in the south, maxima are observed in November (ranging from 200 to 400 mm). During the short dry season, in January and February, precipitation decreases down to 50/200 mm per month in the north/south respectively. From the end of February to May, the active zone of the monsoon flow crosses the basin, usually reinforced by the penetration from the east of humid air masses from the Indian Ocean. This is the second rainy season, with rainfall around 200 mm per month across the ORB.

Two types of natural vegetation are predominant in the ORB: primary forests and savannas. The rainfall abundance accounts for the large biodiversity of the equatorial forest, which is very rich in species. Forests occupy about 80% of the total area of the ORB and savanna trees almost the rest since the rural density of occupation is 1 inhabitant/km² and the agricultural pressure is very low (Braun et al. 2015). Temperatures show little change during the year in the northern and interior regions; the warmest period is from January to May, when the maximum temperature is about 30°C, while from June to September the temperature drops a little, reaching about 24/25°C on the coast, and 27/28 ° C in the interior regions. In the interior hilly regions, the heat is tempered by the altitude.

3. Materials and Methods

3.1 Datasets

3.1.1 Precipitation data

Rainfall analysis in tropical zones is often limited by the insufficient number of datasets available, due to the low number of in situ stations and the numerous gaps in the time series (Arvor et al. 2008). In the ORB, all meteorological stations stopped operating in 1997 (Maloba Makanga 2015). To overcome this lack of data, satellite data can be used to obtain

homogeneous precipitation estimates over the Earth's surface, particularly the oceans and the developing regions (Arvor et al. 2008). The Tropical Rainfall Measuring Mission (TRMM) satellite datasets are one of the most commonly used satellite datasets to characterize rainfall variations in the tropical regions (Barros et al. 2000; Collischonn et al. 2008; Juárez et al. 2009; Franchito et al. 2009; Condom et al. 2011; Scheel et al. 2011; Frappart et al. 2013; Zulkafli et al. 2014; Anders and Nesbitt 2015; Mantas et al. 2015; Erazo et al. 2018). Rainfall data used as forcing for the model from 1998 to 2015 are the TMPA-3B42 V7 daily precipitation product. These data are available at https://pmm.nasa.gov/data-access/downloads, at 0.25° x 0.25° spatial resolution (Huffman et al. 1997).

3.1.2 Land and climatological data

Not only the precipitation data are sorely lacking for the Ogooué basin, but also all other meteorological data are very scarce. In the modeling approach used in this study, forcings were defined using climatic data (climate normals of wind speed, solar radiation, relative humidity, air pressure, and air temperature) provided by the Climatic Research Unit (CRU). The data are long-term climatologies usually used for large river basins, considering that major hydroclimatic changes have not occurred in the basin. The version of the CRU data used here is the CRU 10' long-term climatology data (New et al. 2002).

Land use and land cover information were obtained from ECOCLIMAP, which is a database of continental surface parameters of 1km spatial resolution. The data are largely used to initialize the Soil-Vegetation-Atmosphere-Transfer (SVAT) in weather forecasting and climate models (Masson et al. 2003; Champeaux et al. 2005).

3.1.3 Topography and drainage network

The topography is obtained using a digital elevation model (DEM) from Shuttle Radar Topography Mission (SRTM). The SRTM DEM used in this work is an SRTM 90 m DEM with a resolution of 90 m at the equator. These data are provided in mosaicked 5° x 5° tile for easy download and use. The topography data are available at http://srtm.csi.cgiar.org (Jarvis et al. 2008). All are produced from a seamless dataset to allow easy mosaicking. The drainage network of the ORB is derived from this SRTM DEM using the IPH-HydroTools (it is an IPH made a plugin of the MapWindow GIS and the QGIS for extracting attributes such as drainage line and catchments from digital elevation models) package (Siqueira et al. 2016).

3.1.4 In situ and altimetry-based water levels and discharge

In situ daily water levels of the Ogooué river at Lambaréné (10.2220 °E, - 0.7139 °N) were obtained from the Société de l'Eau et de l'Energie du Gabon (SEEG) for the period July 2001 - September 2017. Altimetry-based time series of water levels were also used in this study. They were obtained using the Multi-mission Altimetry Processing Software (MAPS) (Frappart et al. 2015; Normandin et al. 2018) at four cross-sections called Virtual Stations (VS) between radar altimetry satellite tracks and Ogooué and Ivindo rivers. The radar altimetry missions involved are the 35-day revisit time missions Envisat and Saral Altika for three VSs called here VS_315_Ogooué, VS_272_Ogooué and VS_272_Ivindo, and the 10-day revisit time mission Jason-2 for one VS referred here as VS_185_Ogooué. These altimetry derived water stages were available for periods 2002 - 2010, 2008 - 2016 and 2013 - 2016 for the missions Envisat, Jason-2 and Saral Altika respectively. More details on the processing of the altimetric data can be found in (Bogning et al. 2018). Main characteristics of these VSs are presented in Table 1.

3.1.5 Sea Surface Temperature (SST)

Two SST datasets were used in this work. The first one is the daily 1° X 1° gridded reanalysis SST for the whole tropical area (precisely between 30°N and 30°S) obtained from the European Centre for Medium-Range Weather Forecasts (ECMWF). The ECMWF data can be found at http://www.ecmwf.int/research/era (Dee et al. 2011). The latter dataset was used for analyzing teleconnections between rainfall in the ORB and global SST variabilities especially in the tropical oceans. The second dataset was the monthly 4 km x 4 km gridded remotely sensed SST derived from an hourly Meteosat Second Generation SST data record provided by the Ocean and Sea Ice Satellite Application Facility (OSI SAF) (Saf 2018). It is used for detecting causality between the Ogooué River discharge and coastal Atlantic SST variations in the vicinity of the Ogooué River mouth.

3.2. Data analysis techniques

In this study, two components of the hydrological cycle were analyzed: rainfall and discharge estimated using satellite-based precipitation products and hydrological model outputs respectively. The hydrological model used in this study was calibrated using in situ measured discharges downstream of the ORB and altimetry-based river discharges to face the lack of fields measured data upstream of the ORB.

In addition, the influences of climate mechanisms are investigated using teleconnection analysis in order to detect close and remote forcings and their impacts on detected changes in the river basin. A plethora of indices representing modes of climatic variability is employed in the literature on the teleconnection between climatic and continental hydrology variabilities (Todd and Washington 2004; Singhrattna et al. 2005; Azad and Rajeevan 2016; McGregor 2017; Frappart et al. 2018; Adarsh and Janga Reddy 2019). While these indices have been remarkably helpful in revealing climatic features that underlie some hydrological

variabilities in recent decades, these teleconnections have been more viewed as pure statistics without significant attention given to diagnosing the relationship between climatic mechanisms and hydrological processes. In this study, climate teleconnections are viewed in another lens based on the use of the Empirical Orthogonal teleconnection (EOT) analysis to characterize global tropical monthly anomalies of SST low-frequency variability modes and their influences on the hydrology of the ORB. This approach makes it possible to investigate teleconnections in terms of ocean physics and dynamics.

The impact of the Ogooué river discharge on coastal areas was finally examined using the wavelet cross-correlation between this hydrological flux and the sea surface temperature. The wavelet technique was involved to gain confidence in causal relationships between the Ogooué river discharge and variations of physical parameters of the Ogooué river plume. The whole approach used in this study is summarized in Figure 2.

3.2.1 MGB model description

The MGB ("Modelo de Grandes Bacias" or "Large Basins Model") hydrological model is a semi-distributed process-based model using physical and conceptually based equations to simulate continental hydrological cycles developed by the Large Scale Hydrology research group of IPH-UFRGS (an acronym from the Portuguese for Institute of Hydraulic Research and Federal University of Rio Grande do Sul) (Pontes et al. 2017). The studied river basin is divided into small unit-catchments connected by channels, which are further divided into Hydrological Response Units (HRUs) (Siqueira et al. 2018) that are conceptually produced by areas of similar environmental combination based on geographical information systems data characterizing the basin including topography, vegetation cover, land use and soil type (Collischonn et al. 2008). Then, vertical water and energy balance are computed using

terrestrial components of the water cycle including evaporation, evapotranspiration, soil water budget and runoff for each HRU. Runoff of each HRU of each unit-catchment is summed and routed through the river drainage. The aforementioned components of the water cycle are computed in the MGB model using meteorological data including precipitation, air temperature, relative humidity, wind speed, insolation, and atmospheric pressure (see Figure 3).

3.2.2 MGB model calibration and validation

The calibration procedure of the MGB model was carried out through the optimization of model performances by comparing observed and simulated river discharges. The calibration of the MGB model is evaluated using three performance metrics used as objective functions. The first metric is the Nash and Sutcliffe (1970) criterion or Nash-Sutcliffe Efficiency (NSE) calculated on the streamflow values, the second metric is the Nash-Sutcliffe criterion calculated on the logarithmically transformed flow rates referred here as NSElog and the last one is the volume error called ΔV. If the NSE gives an aggregated measure of how well a modeling hydrograph is close to the observed one in general, the second performance metric puts more emphasis on low-flow modeling in such a way that both metrics complementarily give a clear picture of model performances provided that the calibration data are well selected in space and time. The ΔV gives the average percentage departure from the observed discharges.

In general, longer period calibrated continuous rainfall-runoff hydrology models are considered more robust and reliable as they are likely to take into account various hydrological processes of the interested river basin (Perrin et al. 2007). To some extent, using the full period of observed data available for hydrology model calibration can be deemed to satisfactorily reproduce all hydrological behaviors of the interested river basin over the

modeling period. However, beyond the limitation of the feasibility of such hydrology models for their solely observed period, longer period calibrated hydrology models may require significant computational efforts to replicate related river basin parameters (Razavi and Tolson 2013). Thus, the determination of an efficient short period of observed data for the calibration of hydrology models is fundamental.

It is often a challenging task to determine a short period of data embedding enough information to be sufficiently representative of a long-term observed dataset. In addition, aforementioned in situ and altimetry derived data of the ORB are available neither at the same period, nor at the same sampling period for all considered stations. Due to the periods of simultaneous availability of the different datasets at all stations, the selected calibration period is 07-2008 to 09-2010. The calibration/validation dataset was composed of river discharges estimated at Lambaréné gauge station, and derived from the following radar altimetry missions Jason-2 for the station VS_185_Ogooué and Envisat for both VS_272_Ogooué and VS_272_Ivindo. The validation procedure was performed using the comparison of remaining observed discharge datasets and simulated discharges at all stations. Overall, it should be noted that while the calibration and validation of the MGB model require stream flows, the available in situ measurements and altimetry-derived data are only water levels and should be converted into stream flows. Fortunately, an updated calibration curve for the Lambaréné station was made available by HydroScience Montpelier (HSM), and even if the gauging was not done upstream of the ORB, the rating curves from the databases of the "Office de la Recherche Scientifique et Technique Outre-Mer (ORSTOM)", which is now replaced by "Institut de Recherche pour le Développement (IRD)" were used. However, since altimeters do not generally cross rivers at locations monitored in fields, linear regression can be done to convert the data acquired by the altimeters at a few tens of kilometers from the station in situ provide that hydrodynamic conditions are expected to be

quite similar between the two points as there is neither large tributaries nor large floodplains between them. Water stages are thus converted into river discharges using de the following equation (Papa et al. 2012; Bogning et al. 2018):

$$Q(t) = \alpha(h(t) - h_0)^{\beta} \quad (1)$$

where $Q(t)$ is the instantaneous river discharge, $h(t)$ is the instantaneous water stage, h_0 the null-discharge elevation, and α and β are related to the geometry of the channel cross-section and to the friction coefficient modulating the discharge. h_0 is adjusted in order to keep mean discharges close considering that major hydrodynamic changes do not occur.

3.2.3 Time series of monthly rainfall

For a given basin of surface area S, the average rainfall δh of a given month t is computed based on the equation (2) below developed in (Ramillien et al. 2006)

$$\delta h(t) = \frac{R_e^2}{S} \sum_{j \in S} h(\lambda_j, \theta_j, t)\, sin\theta_j\, \delta\lambda\delta\theta \quad (2)$$

where h_j is local monthly rainfall, with $j = 1, 2, 3, ...$, expressed in mm per month, λ_j and θ_j are longitude and co-latitude, $\delta\lambda$ and $\delta\theta$ are the grid steps in longitude and latitude (generally $\delta\theta = \delta\lambda$, S is the surface area of the basin and R_e the mean radius of the Earth ~6371 km)

3.2.4 STL decomposition

The Seasonal and Trend decomposition using LOWESS (STL decomposition) of a time series is a versatile and robust method for decomposing a time series $h(t)$, into seasonal $S(t)$, trend $T(t)$, and residual $R(t)$ components using a non-parametric approach (Cleveland et al. 1990) such that:

$$h(t) = S(t) + T(t) + R(t) \quad (3)$$

The STL decomposition method, based on locally weighted regression, is used for detecting non-linear patterns in trend estimates. In this study, the STL decomposition was applied on the time series of rainfall and river discharges of the ORB for the analysis of overall

variations of rainfall and runoff in the ORB on one hand and the determination of underlying factors governing these variations on the other hand.

3.2.5 Empirical orthogonal teleconnection

EOT analysis was used to identify spatial patterns with coherent interannual rainfall variability in the ORB and their relationships with global tropical SST. EOT analysis was first introduced by (van den Dool et al. 2000) as an alternative to empirical orthogonal functions (EOFs) analysis to reduce abstracted results very often associated with the latter (Appelhans and Nauss 2016). Time series of SST anomalies in the global tropics, termed the domain predictor, are analyzed in regard to the explained variance of time series rainfall anomalies in the ORB termed the response domain. EOT was computed following the algorithm presented in (Appelhans and Nauss 2016) using the "remote" package implemented in open-source software R (Appelhans et al. 2015). Monthly average 1° X 1° gridded global tropical SSTs have been used as the predictor series and monthly 0.25° X 0.25° gridded TRMM precipitation data over the ORB were used as the response domain. Instead of orthogonality in time and space that governs EOF analysis, EOT analysis is orthogonal either in time or space which makes it less constraining and easier to implement, providing that both the predictor and the response time series span the same period.

3.2.6 Wavelet cross-correlation and coherence

Wavelet cross-correlation was applied to time-series of river discharge at Lambaréné and of SST in the Ogooué coastal area to identify the temporal scales presenting similar variations in these two-variables. Thus, the cross-wavelet power spectrum of both variables was computed in order to depict its time-frequency space relationships trough wavelet cross-spectrum peaks in the periodogram. This technique has been used by numerous authors in climatology

(Torrence and Webster 1999) and environmental sciences (Labat et al. 2000; Pozo-Vázquez et al. 2001; Vu et al. 2019). However, some peaks in the cross-spectrum have nothing to do with any relation of the two variables (Torrence and Compo 1998). Thus, the significance of the results was checked using the wavelet coherence. All computational processes related to the wavelet technique were performed in this study using the software package available at www.pol.ac.uk/home/research/waveletcoherence/ (Grinsted et al. 2004).

4. Results

4.1. Rainfall variability analysis

The annual distribution of rainfall in the ORB is shown in Figure 4 from 2000 to 2015. The ORB receives a large amount of precipitation with annual rainfall varying from more than 1000 mm to less than 3000 mm/year. Two decrease rainfall gradients can be observed: one eastward, from the coast to the mainland and the other northward. The lower amount of rainfall in the northern part of the basin is due to its location crossing the Equator (Maloba Makanga 2015). The time series of basin-scale monthly precipitation is presented in Figure 5a. It shows a bimodal precipitation pattern with maxima occurring between March and May (low rainy season), September and October (large rainy season). Nevertheless, it should be kept in mind that the dry season is not a total disappearance of precipitations over the ORB, but a significant decrease in rainfall. In fact, hundreds of millimeters of precipitations are recorded in the ORB during the two dry periods, as shown in Figure 5b showing the monthly average rainfall in the ORB. In turn, inter-annual variability of rainfall in the ORB is really moderate over the study period in spite of important local differences (see Figure 4). In fact, the standard deviation of the basin-scale annual precipitation time series is 181.9 mm for the study period, i.e. 8.14 % of the maximum recorded averaged precipitation.

4.2. Results of model calibration and validation

The resulting values of these metrics for the calibration performed in the ORB are found in Table 2. The values of these performance metrics suggest that the MGB model well efficiently identified the hydrological behavior of the ORB as NSE ≥ 0.66 for all calibration stations. This is all the more true as the NSElog are all higher than 0.51, indicating that low-flow variations which are often difficult to capture have been well reproduced. The ΔV also confirms the efficiency of the MGB model suggested by the first two assessment criteria (NSE and NSElog) as its values do not exceed 12 % for all the calibration stations.

In addition, as the use of the historical rating curves in altimetry derived calibration data stations can cause uncertainties in the modeling processes, the analysis of the covariation of observed water stages and simulated discharges have been done. The results of this analysis are shown in Figure 6. The consistent values of both coefficients of correlation and determination obtained enhance the MGB model efficiency drawn by the aforementioned assessment criteria with r-square > 0.69 for all the stations. Except for the observed-simulated data pairs of the station VS_272_Ivindo which can be considered sparse, the scatterplots of other stations are harmonious on both sides of the linear regression and may take into account significant hydrological information.

The performance of the MGB model is estimated through the comparisons of simulated and observed discharges outside of the calibration period. These comparisons are shown in Figure 7. The satisfactory results obtained over the calibration period is visibly extended out of this period as a close agreement is found between simulated and observed streamflow curves represented for all assessed stations. The model provides realistic simulations of the annual variations of the discharge of the Ogooué River which displays two maxima: in spring and autumn corresponding to the rainy seasons. This indicates that the MGB model reliably estimated water balance in HRU and efficiently replicated the hydrological processes in the

ORB. These results also demonstrate the robustness of calibration data as it provides sufficient information for a good replication of main hydrological behaviors of the ORB. The present MGB modeling procedure can be equally deemed parsimonious taking into account the short period length of observations used for the calibration. Indeed, apart from the Lambaréné gauge station located downstream of the ORB where almost 2-year daily observations were involved, only some tens of observations were available for upstream stations. In contrast to some studies which proposed that the difficulties of the calibration processes are overcome provide that almost 350 daily observations (Perrin et al. 2007) or at least 2-year continuous recorded data (Juston et al. 2009) are used, this study points out that no required period length of observations can be generalized. The most important requirement is the diversity of hydrologic information contained in the observed data which should be sufficient to appropriately replicate hydrologic variability in the river basin.

However, some discrepancies are observed in the prediction of streamflow in extreme conditions, especially when high streamflow values are considered. The MGB model underestimated streamflow maxima as it can be seen in the comparison of simulated with in situ measured as well as altimetry derived discharges downstream and upstream of the ORB respectively.

4.3. Consistency between rainfall and river discharges in the ORB

The time series of monthly rainfall were computed over the drained surface monitored by the gauge stations where the calibration and the validation of the MGB model were performed in the ORB. In order to analyze the relationship between rainfall and runoff in the ORB, cross-correlation of both time series of rainfall and river discharges were computed on the original series and their interannual variations obtained using the STL decomposition. Table 3 shows the maximum values of the cross-correlation between the time series of rainfall and river discharges and corresponding time-lag. The maximum values of cross-correlation between

the total time series of rainfall and river discharges are all higher than 0.8 and the one-month time-lag for the maximum correlation is the response time of the ORB to rainfall. This good agreement is in accordance with our knowledge of the hydrological regimes of rivers in the equatorial zone where river discharges are generally closely related to discharges at the annual time-scale (Bricquet 1990).

The maximum values of the cross-correlation of the STL decomposition trend components of both time series of rainfall and runoff are also shown in Table 3. High correlations, ranging from 0.72 to 0.95 with no time-lag, are observed between rainfall and discharge at an interannual time-scale in the ORB, except in the Ivindo Basin where the correlation is only 0.55. This rather low correlation at the interannual time-scale is most likely due to the lower performances of the coupled remote sensing/modeling approach in the Ivindo Basin (see 4.2). If these lower performances have a low impact on the whole time series as a strong seasonal signal is observed in the ORB, it negatively affects the discharge estimates at an interannual time-scale. Thus, all changes observed on the trend components of the time series of rainfall and river discharges (Figure 8) should be related to natural phenomena influencing rainfall and consequently runoff in the ORB. Anthropogenic inferences (e.g., water abstraction, crop irrigation, logging, and even mining) have no significant impact on water resources of the basin over the study period, in good agreement with the status of a well-preserved river basin usually conferred to the ORB (Sannier et al. 2014; Braun et al. 2015).

Interannual variability of rainfall and discharge were also analyzed using STL decomposition. The STL decomposition trend components of the time series of rainfall over the drainage area delimited downstream by a discharge measurement and the corresponding river discharge trend components are presented over the study period in Figure 8 for the four considered stations. Interannual co-variations of rainfall and river discharge hardly differ over the entire basin. This suggests a strong spatial coherence in temporal variations of rainfall and also of

river discharge in the ORB at the interannual timescale. However, seasonal curves resulting in STL decomposition (not shown because of brevity) exhibit a singular variability compared to other stations of the basin in rainfall as well as in river discharge.

4.4. Rainfall forcings of the ORB

Rainfall variabilities in western-central equatorial Africa including the ORB is characterized by extreme heterogeneity at the interannual scale which is in contrast with other regions in Africa (Nicholson 1986; Balas et al. 2007; Nicholson and Dezfuli 2013). This heterogeneity has been interpreted as a result of complex interacting mechanisms among various atmospheric, oceanic and static geographical features, influencing from regional to global scales (Balas et al. 2007; Dezfuli 2017). Regarding the ORB, the basin area is located at the coastal part of western central equatorial Africa mostly influenced by local SST anomalies (Nicholson and Dezfuli 2013; Dezfuli and Nicholson 2013) and remotely forced by the global atmospheric circulation in the tropics which is strongly linked to SST conditions in the three main ocean basins (Balas et al. 2007; Dezfuli 2017). In order to understand how rainfall variabilities in the ORB are affected by global tropical SST anomalies, EOT analysis was applied to 1998 - 2015 precipitations and 1° X 1° global tropical SSTs.

Figure 9 shows the first two modes of EOT analysis of the association between rainfall variability in the ORB and global tropical SST anomalies. The EOT technique was used to decomposed SST fields into a set of independent and orthogonal patterns based on the scale of the calculated coefficients of determination based on the regression of the SST time series against the time series of rainfall the ORB. The first EOT mode (Figure 9a) exhibits a pattern of SST anomalies in the southeastern equatorial Atlantic Ocean especially along Angolan, Congolese and Gabonese coasts and an extension forward into the Atlantic cool tongue materialized by high values of the determination coefficient. It is positively correlated to rainfall in the ORB, especially in the southern part of the basin. This is in good agreement

with some previous studies (Nicholson and Dezfuli 2013; Dezfuli and Nicholson 2013; Nicholson et al. 2018) which denoted strong links between rainfall in the coastal part of western equatorial Africa and local SST variations. In turn, the second mode (Figure 9b) revealed the influences of the Pacific basin which is observed on its western part as a pattern of high coefficients of determination. This mode confirms the relationship - negative correlation - between El Nino Southern Oscillation (ENSO) in the equatorial Pacific basin and rainfall variability in the ORB. The latter result was also recently obtained by several authors(Balas et al. 2007; Nicholson and Dezfuli 2013; Dezfuli and Nicholson 2013; Maloba Makanga 2015; Dezfuli 2017). In this second mode, one can also notice that the pattern of coefficients of determination is not very high in the Indian Ocean,with values lower than 0.6. This does not necessarily suggest a strong link between rainfall variations in the ORB and SST anomalies in this ocean basin, although it should be kept in mind that SST in the tropical Indian Ocean basin influences global atmospheric circulation that rainfall in ORB depends on.

For both modes presented in Figure 9, the absolute values of resulting correlation coefficients in the ORB do not exceed 0.4. The relatively low correlation values come from the fact that rainfall beyond SST depends on a multiplicity of atmospheric and local factors. The opposite signs of correlation coefficients for the two modes show that SST variations in the southeastern tropical Atlantic and the equatorial Pacific differently affect rainfall heterogeneity in the ORB. To summarize, this suggests that increasing SST in the southeastern tropical Atlantic (equatorial Pacific) results in increasing (decreasing) heterogeneity of rainfall in the ORB. Nevertheless, it should be noted that the above results have shown that rainfall is consistent throughout the ORB.

4.5. Ogooué River plume in the Atlantic Ocean

The Ogooué River discharge provides a large amount of freshwater into the Atlantic in Cap Lopez which may have significant effects on the physical properties of seawater in this region. Recently, Mignard et al. (2017) stated that freshwater outflow from the Ogooué River into the Atlantic Ocean stretches as far as 100 km up to Sao Tomé Island. This outflow can be detected through a reduced salinity water layer of about 20 m thick. In general, beyond Sea Surface Salinity (SSS) variations, river discharges in oceans also impact SST, pollution, carbon, nutrients and, other physical and biogeochemical properties of the local ocean (Witman 2017). Yet, the determination of the dynamics of river plumes in the coastal seas and oceans is generally a real challenge, and the case of the Ogooué River is no exception given that several rivers also discharge large amounts of freshwater in the Atlantic Ocean not far from the Ogooué River mouth among which the Congo River, which is the second largest rivers in the world in terms of river discharge. During the peak flow, Congo river discharge is likely to reach eight times the discharge of the Ogooué River.

Another major reason that makes it difficult to understand variational processes in river plume properties is the lack of reliable measurements of physical and biogeochemical parameters at reasonable spatial and temporal scales in coastal oceans to capture variability patterns and the factors these latter depend on. In the vicinity of the Ogooué River mouth, only remotely sensed SST data are available for a relatively long period in order to analyze the relationship between the Ogooué River discharge and SST at its mouth. Considering that the SST and river discharge time series may contain the non-stationary power at different frequencies, time-resolved wavelet coherence analysis (Grinsted et al. 2004; Maraun and Kurths 2004) was used for investigating causality between both time series. Because the Ogooué River plume has been detected as far as the Sao Tomé Island, the Ogooué River plume was defined in an area located between 6°E - 9.5°E and 2.5°S - 1°N.

Figure 10 shows the result of the cross wavelet spectrum and wavelet coherence between the

Ogooué River discharge and the spatially average time series of SST in the mouth of the Ogooué River. Time-frequence areas of significant cross wavelet are delineated inside the areas of high power magnitude and outlined by the thin black lines. Two delineated power peaks are observed in the cross-correlation wavelet spectrum (Figure 10a) around the 6th month and the 12th month period denoting a strong correlation between both time series at these periods. However, a peak in the cross wavelet spectrum might arise either because of the structure of a particular time series or due to the interaction between both time series (Kumar and Foufoula-Georgiou 1997). Thus, the wavelet coherence (Figure 10b) was used to confirm the significance of the cross-correlation at both periods and almost over the full study period as both periods are inside the zones outlined by the thin black lines. The observed structures correspond to the annual and semi-annual components of the Ogooué river discharge which modulates accordingly to the SST. The latter periods deal with the high flooded seasons of the Ogooué River that do certainly have important impacts on Atlantic ocean water properties in the Ogooué River mouth.

5. Discussion

5.1. Hydrological modeling of the ORB through a satellite-model coupled approach

Combinations of hydrological modeling and satellite observations are increasingly used to offset the decrease of in situ hydrological networks around the world for both scientific and water management purposes. Their interest for researchers as well as for decision-makers is growing owing to their ability to predict the spatial and temporal variation of river basin hydrological processes, which is improving at local and global scales (Sood and Smakhtin 2015; Paris et al. 2016; Fleischmann et al. 2018). The MGB model was used to simulate long-term discharge variability in the ORB during the last two decades based on the resolution of the water and energy budget in each defined HRU. Overall, a close agreement

was found between MGB simulated river discharges and in situ and altimetry derived ones as NSE ≥ 0.66 at all assessed points of the basin. Obviously, better simulations were obtained downstream of the ORB at Lambaréné (NSE = 0.76). Even though the comparison was made using in situ measured discharges, a long-term multimission altimetry-based discharge was compared to these in situ data and close agreements were found between both time series with r = 0.93 and relative error = 0.03 % (Bogning et al. 2018). In the ORB,assuming that the stage-discharge rating curves remain valid (i.e. assuming no change in the hydrological regime caused by climate or anthropogenic factors such as dam buildings, deforestation affecting rainfall and runoff, or in the river wet section), discharge monitoring could be ensured using VS from altimetry multi-mission (currently Jason-3, Sentinel-3A and B) if the Lambaréné gauge station is not operational anymore. Otherwise, the calibration of MGB could be performed using altimetry-based water stages.

It should be noted that in this work, the calculation of all process components represented in the MGB model describing the conceptualized HRU presented in Figure 3 were not explicitly detailed. However, the consistency in terms of correlation between rainfall and river discharge at each calibration/validation point at seasonal ($r > 0.8$ in all cases) and inter-annual ($r > 0.8$ for three of the four cases) scales demonstrate a satisfactory replication of the spatio-temporal variations in river discharges by the MGB model throughout the ORB. Moreover, one can deduce from the above coherence that the terrestrial water cycle in the ORB has not changed much over the study period as the stage-discharge relationship remained valid over several decades. This indicates good preservation of the ORB ecosystem as deforestation can considerably affect the hydrologic cycle based on variations in precipitation, evapotranspiration, moisture convergence and probably runoff, along with increments in surface temperature (D'Almeida et al. 2007).

The calibration curves used to convert the water levels into discharges were obtained from historical measurements and probably changed as the river bed evolves. These rating curves were updated using the simulated discharges and both in-situ and satellite altimetry water levels (Figure 11) in order to improve the river discharge estimations in the ORB, following the methodology presented in Paris et al. (2016). These rating-curves provide reliable estimates of river discharges in the entire ORB (NSE $\geq$ 0.52 in all cases and up to 0.8 in Lambaréné not far from the mouth of the ORB) although better results are found downstream rather than upstream where 1) the small river width and the presence of topography are impacting our capacity to retrieve accurate water level time series and 2) the simulated discharges may not represent some short time or space-scale precipitation events. Besides, larger uncertainties in the conversion of recorded river stages into discharge (measurement uncertainty) comes from larger gauging errors in the upstream part of the rivers (Tomkins 2014). Beyond measurement and rating curve uncertainties, a larger number of the recorded stage - flow pairs lead to better characterization of stage and flow co-variations and hence a more representative empirical relationship between river stages and flows as it is shown in Figure 11. Moreover, instantaneous water surface stage-discharge pair points are grouped around an average rating curve over the entire assessing period, which shows the consistency of these curves and makes them new empirical relationships that could possibly be used for the evaluation of flow rates from water stages. Moreover, these rating curves would enable the near real-time monitoring of the evolution of river discharges in the ORB using the Operational Geophysical Data Record (OGDR) products from the current altimetry missions (e.g. Jason-3, Sentinel-3A and B) or from newly installed or restored in situ gauge stations in close vicinity of a VS. For instance, in the context of the restoration of the gauge station of Lambéréné destroyed in December 2017 during an extreme event, the in situ and altimetry

derived rating curves in Lambaréné could be used to generate river discharges from water stages.

5.2. Relationship between rainfall and SST in ocean basins

The EOT analysis has allowed the identification of the teleconnections that influence the precipitation in the ORB through the SST. Two major oceanic regions were particularly identified in the southeastern tropical Atlantic Ocean and the eastern central Pacific Ocean. Nevertheless, this analysis is not sufficient (and beyond the scope of this study) to quantify these impacts. If the mechanisms governing SST variations in the eastern and central Pacific are well documented (An and Wang 2001; Santoso et al. 2017; Yun et al. 2019), those of the eastern tropical Atlantic basin are less known despite some notable endeavors (Camberlin et al. 2001; Lutz et al. 2013; Exarchou et al. 2018). A brief insight of SST in the tropical Atlantic based on the bulk of the related literature revealed that the ocean and climate conditions of the southeast part of this region are really similar to those of the southeast tropical Pacific in Peruvian coasts (Hisard 1990; Nicholson and Entekhabi 1987). The southeast tropical Atlantic experienced anomalously high SSTs in the interannual scale, about every 3 to 5 years (Lutz et al. 2015). Another sporadic interannual fluctuating SST gradient is centered in the equatorial Atlantic (Carton et al. 1996; Nnamchi et al. 2015). Based on the analogy with Pacific dynamics, these warm-water events of the tropical Atlantic have been termed Niño events, the equatorial one is the Atlantic Niño (Zebiak 1993; Okumura and Xie 2006; Nnamchi et al. 2015) and southeast tropical coastal ones have been termed Benguela Niño events (Shannon et al. 1986; Lutz et al. 2013). The so-called Atlantic and Benguela Niños have long been perceived as independent events and analyzed separately. However, Lübbecke et al. (2010) found a high correlation between the eastern equatorial Atlantic and Benguela SST anomalies in boreal spring showing the association between the eastern equatorial Atlantic and Benguela warm events and suggesting that both Atlantic and

Benguela Niños are two parts of the same phenomenon. In addition, (Lutz et al. 2013) found significant correlations of SST anomalies recorded in three delineated areas spanning the tropical Atlantic connecting the Benguela coast to the equatorial Atlantic area demonstrating the spatial continuity of warming from the Benguela coast to the Atlantic cool tongue. This combination of the Atlantic Niño and the Benguela Niño was named the tropical Atlantic Niño.

Regarding the ORB, the hydrological cycle and the origin of driving factors of its changes have not been convincing investigated recently. Although some authors, based on studies over continental (Nicholson et al. 2018) or regional (Balas et al. 2007; Nicholson and Dezfuli 2013; Dezfuli and Nicholson 2013; Hua et al. 2016) areas including the ORB argued strong relationships between rainfall in western equatorial Africa and SST anomalies in the southeastern tropical Atlantic and the equatorial Pacific, no significant correlation is found between rainfall anomalies in ORB and ENSO and tropical Atlantic Niño indices over the study period. This suggests that, although rainfall in the ORB strongly depends on tropical SST anomalies as it is a monsoon area, these dependencies vary with respect to seasons which is consistent with (Hua et al. 2016; Nicholson et al. 2018). Nevertheless, concerning the central Pacific, the influences of rainfall generally associated with ENSO lie in a reduced effect when El Niño occurs (Maloba Makanga 2015; Gizaw and Gan 2017). However, are precipitations strengthened in western equatorial Africa when la Niña occurs? Moreover, given the simultaneous occurrence of ENSO and Atlantic Niño, estimating the individual influence of each phenomenon on rainfall in the ORB is a really challenging task.

The seasonal distribution of rainfall in the ORB based on a long-term time series of rainfall measurements is such that the cumulative rainfall in September-November (SON) is 37% of the annual total of the river basin, compared with 33% for the rainy season of March-May (MAM) with the small dry season of December-February (DJF) collecting 26% of the total

annual rainfall while the water levels of the main dry season of June-August (JJA) barely reach 4% (Maloba Makanga 2015). This latter distribution clearly shows the rainfall deficit of boreal springs observed since the 1970s (Nicholson et al. 2018; Dieulin et al. 2019) which highlights a different evolution of Spring and Autumn floods in the ORB (Lienou et al. 2008; Mahé et al. 1990). This decline of MAM rains was related to the poor rainfall conditions of the monsoon flux during the northern migration of the ITCZ (Citeau et al. 1989; Mahé et al. 1990), corroborated by SST anomalies and equatorial upwelling (Mahé and Citeau 1993). Considering that the MAM season is the most sensitive, investigations of its dependence on influencing tropical ocean basins have been made using the EOT analysis. Figure 12 shows the co-evolution of MAM rainfall in the ORB with ENSO (Niño34 index) in DJF and tropical Atlantic Niño in JFM. It can be seen that negative anomalies of SST in the southeastern equatorial Atlantic in JFM result in positive anomalies of rainfall in MAM in the ORB. In contrast, MAM negative anomalies of rains in the ORB mainly occurred following combined warming in the central Pacific and the southeastern equatorial Atlantic basins in DJF and JFM respectively. Correlation between rainfall anomalies in the ORB and ENSO in DJF and tropical Atlantic Niño in JFM indices were estimated. For tropical Atlantic Niño in JFM, r = -0.741 with p-value = 0.00042; whereas for ENSO in DJF, r = -0.212 with p-value = 0.397. One can see from the correlation values that tropical Atlantic Niño influenced rainfall in MAM in the ORB over the study period. Inversely, no relationship can be found between ENSO in DJF and rainfall in MAM in the ORB. Thus, this does not lead to any conclusion over the study period, especially since no major El Niño event occurred during the study period except for the year 1998 which shows nevertheless a significant deficit in rainfall. The negative sign of these correlation values underlies the inverse variations of rainfall in the ORB and SST in both ocean basins in the respective selected periods.

In summary, SST anomalies in both ocean basins play a leading role in inter-annual rainfall variability in the ORB as it has been shown using the EOT analysis with more pronounced effects for the eastern equatorial Atlantic. Moreover, it should be noted that if some authors suggest that rainfall in tropical region may increase by taking advantage of global warming and hence land-sea thermal gradient in the tropics (Chou 2003; Sutton et al. 2007; Wu et al. 2012), rainfall is favored in the ORB and surrounding areas by cooling conditions in the ocean basins and that is consistent with (Hua et al. 2016; Nicholson et al. 2018). And it may be hypothesized that the warming trend of the tropical oceans will lead to a deficit of rainfall and consequently a reduction of river discharges in the ORB and the surrounding basins.

6. Conclusion

This study is twofold: i) altimetry-based river discharges were used to calibrate the MGB hydrological model for estimating river discharges in the poorly gauged ORB, ii) temporal changes of rainfall and discharges were analyzed over 1998-2015 in this basin. Using altimetry-derived water stages from ENVISAT and Jason-2 at three cross-sections of the altimetry ground-tracks and the Ogooué River and its major tributary and the gauge records from the Lambaréné station, calibration and validation of the MGB model was achieved. For instance, at Lambaréné downstream of the ORB, not far from the mouth of the Ogooué river in the Atlantic Ocean, the closest match of river flow variations were found (NSE = 0.76, NSElog = 0.81) and especially, model and in situ measured river discharges only differ by 0.70 %. Even if the results were sometimes less consistent upstream, they were satisfactory with NSE $\geq$ 0.66 and NSElog > 0.51 for the three cross-section VSs analyzed.

Close co-variations between rainfall and river discharge at each calibration/validation point at seasonal ($r \geq 0.72$ in all cases) and inter-annual ($r > 0.8$ for three of the four cases) scales demonstrate a satisfactory simulation of the hydrological processes by the MGB model throughout the ORB and not much changes in terrestrial water in the ORB over the study

period. In addition, the EOT analysis clearly relates the variations of rainfall in the ORB to changes in the SST conditions in the eastern and central equatorial Pacific Ocean and the southeastern equatorial Atlantic Ocean. A correlation value of -0.741 was found between rainfall in MAM in the ORB and tropical Atlantic Niño index demonstrating the leading role of the southeastern tropical Atlantic SST anomalies on rainfall variations in the ORB. In addition, it has been shown that cool events in the latter ocean basin induced increased rainfall in the ORB whereas warming conditions lead to a rainfall deficit. Globally, rainfall and hence water resources in the ORB are thereby modulated by tropical Atlantic Niño and ENSO.

Moreover, one of the major interests in the ORB nowadays is to relaunch general monitoring of the basin to address research and management issues. The MGB modeling of the ORB has produced a crucial database of hydrological data that could be useful both for scientific researches and for decision making, and thus promoting the implementation of sustainable development policies throughout the ORB.

7. Acknowledgements

This work is part of three projects: the Laboratoire Mixte International (LMI), Dynamique des écosystèmes continentaux d'Afrique Centrale en contexte de changements globaux (DYCOFAC), the French national programme EC2CO-Biohefect "Régime d'Altération/Érosion en Afrique Centrale (RALTERAC)" and the CNES/TOSCA CTOH project. The authors are grateful to the Center for Topographic studies of the Ocean and Hydrosphere (CTOH) at LEGOS (Toulouse, France) for providing the altimetry dataset. We also thank the Lambaréné branch of the Société de l'Énergie et de l'Eau du Gabon (SEEG) (Lambaréné, Gabon) for supplying the Ogooué water level from the Lambaréné hydrological station. Further thanks go to the "Service Coopération et de l'Action Culturelle (SCAC)" of

the French Embassy in Cameroon and TNC-Gabon. Final acknowledgments are for the project “Jeune Equipe Associée à l’IRD—Réponse du Littoral Camerounais aux Forçages Océaniques Multi-Échelles (JEAI-RELIFOME)” from the University of Douala. We want to thank two anonymous Reviewers who helped us improving the quality of our manuscript.

8. References

Adarsh, S., Janga Reddy, M., 2019. Links Between Global Climate Teleconnections and Indian Monsoon Rainfall, in: Venkataraman, C., Mishra, T., Ghosh, S., Karmakar, S. (Eds.), Climate Change Signals and Response: A Strategic Knowledge Compendium for India. Springer Singapore, Singapore, pp. 61–72.

Anders, A.M., Nesbitt, S.W., 2015. Altitudinal Precipitation Gradients in the Tropics from Tropical Rainfall Measuring Mission (TRMM) Precipitation Radar. J. Hydrometeorol. 16, 441–448.

An, S.-I., Wang, B., 2001. Mechanisms of Locking of the El Niño and La Niña Mature Phases to Boreal Winter. J. Clim. 14, 2164–2176.

Appelhans, T., Detsch, F., Nauss, T., Others, 2015. Remote: empirical orthogonal teleconnections in R. J. Stat. Softw. 65, 1–9.

Appelhans, T., Nauss, T., 2016. Spatial Patterns of Sea Surface Temperature Influences on East African Precipitation as Revealed by Empirical Orthogonal Teleconnections. Front. Earth Sci. 4, 3.

Arvor, D., Dubreuil, V., Ronchail, J., Simões Penello Meirelles, M., 2008. Apport des données TRMM 3B42 à l’étude des précipitations au Mato Grosso (Contribution of the TRMM 3B42 data to the study of Mato Grosso precipitations). Climatologie 5, 49–69.

Azad, S., Rajeevan, M., 2016. Possible shift in the ENSO-Indian monsoon rainfall relationship under future global warming. Scientific Reports 6, 20145. https://doi.org/10.1038/srep20145

Balas, N., Nicholson, S.E., Klotter, D., 2007. The relationship of rainfall variability in West Central Africa to sea-surface temperature fluctuations. Int. J. Climatol. 27, 1335–1349.

Barros, A.P., Joshi, M., Putkonen, J., Burbank, D.W., 2000. A study of the 1999 monsoon rainfall in a mountainous region in central Nepal using TRMM products and rain gauge observations. Geophys. Res. Lett. 27, 3683–3686.

Biancamaria, S., Frappart, F., Leleu, A.-S., Marieu, V., Blumstein, D., Desjonquères, J.-D., Boy, F., Sottolichio, A., Valle-Levinson, A., 2017. Satellite radar altimetry water elevations performance over a 200 m wide river: Evaluation over the Garonne River. Adv. Space Res. 59, 128–146.

Biancamaria, S., Schaedele, T., Blumstein, D., Frappart, F., Boy, F., Desjonquères, J.-D., Pottier, C., Blarel, F., Niño, F., 2018. Validation of Jason-3 tracking modes over French rivers. Remote Sens. Environ. 209, 77–89.

Bogning, S., Frappart, F., Blarel, F., Niño, F., Mahé, G., Bricquet, J.-P., Seyler, F., Onguéné, R., Etamé, J., Paiz, M.-C., Braun, J.-J., 2018. Monitoring Water Levels and Discharges Using Radar Altimetry in an Ungauged River Basin: The Case of the Ogooué. Remote Sensing 10, 350.

Braun, J.J., Jeffery, K., Koumba Pambo, A.F., 2015. CZO perspective in Central Africa: The Lopé watershed, Lopé National Park, Ogooué River basin, Gabon. Poster presentation at the AGU Fall Meeting.

Bricquet, J.-P., 1990. Régimes et bilans hydrologiques de l'Afrique Centrale: les apports à l'océan, du golfe du Biafra à la Pointa do Dande (Water regimes and water balances in Central Africa: inputs to the ocean from the Gulf of Biafra to Pointa do Dande), In Lanfranchi, R. and Schwartz, D. (Eds.), Paysages quaternaires de l'Afrique centrale atlantique (Quaternary

landscapes of Central Atlantic Africa). ORSTOM, Paris, pp 42-51..

Camberlin, P., Janicot, S., Poccard, I., 2001. Seasonality and atmospheric dynamics of the teleconnection between African rainfall and tropical sea-surface temperature: Atlantic vs. ENSO. International Journal of Climatology 21, 973-1005. https://doi.org/10.1002/joc.673

Carton, J.A., Cao, X., Giese, B.S., Da Silva, A.M., 1996. Decadal and Interannual SST Variability in the Tropical Atlantic Ocean. J. Phys. Oceanogr. 26, 1165–1175.

Champeaux, J.L., Masson, V., Chauvin, F., 2005. ECOCLIMAP: a global database of land surface parameters at 1 km resolution. Meteorol. Appl. 12, 29–32.

Chou, C., 2003. Land–sea heating contrast in an idealized Asian summer monsoon. Clim. Dyn. 21, 11–25.

Citeau, J., Bergès, J.-C., Demarcq, H., Mahé, G., 1988. The watch of ITCZ migrations over the tropical Atlantic Ocean as an indicator in drought forecast over the Sahelian area. Tropical Ocean-Atmosphere Newsletter 45, 1–3.

Citeau, J., Finaud, L., Cammas, J.P., Demarcq, H., 1989. Questions relative to ITCZ migrations over the tropical Atlantic ocean, sea surface temperature and Senegal River runoff. Meteorol. Atmos. Phys. 41, 181–190.

Cleveland, R.B., Cleveland, W.S., McRae, J.E., Terpenning, I., 1990. STL: A Seasonal-Trend Decomposition. J. Off. Stat. 6, 3–73.

Collischonn, B., Collischonn, W., Tucci, C.E.M., 2008. Daily hydrological modeling in the Amazon basin using TRMM rainfall estimates. J. Hydrol. 360, 207–216.

Collischonn, W., Allasia, D., da Silva, B.C., Tucci, C.E.M., 2007. The MGB-IPH model for large-scale rainfall—runoff modelling. Hydrol. Sci. J. 52, 878–895.

Condom, T., Rau, P., Espinoza, J.C., 2011. Correction of TRMM 3B43 monthly precipitation data over the mountainous areas of Peru during the period 1998-2007. Hydrological Processes 25, 1924-1933. https://doi.org/10.1002/hyp.7949

D'Almeida, C., Vörösmarty, C.J., Hurtt, G.C., Marengo, J.A., Dingman, S.L., Keim, B.D., 2007. The effects of deforestation on the hydrological cycle in Amazonia: a review on scale and resolution. Int. J. Climatol. 27, 633–647.

Dee, D.P., Uppala, S.M., Simmons, A.J., Berrisford, P., Poli, P., Kobayashi, S., Andrae, U., Balmaseda, M.A., Balsamo, G., Bauer, d. P., Others, 2011. The ERA-Interim reanalysis: Configuration and performance of the data assimilation system. Quart. J. Roy. Meteor. Soc. 137, 553–597.

Dezfuli, A., 2017. Climate of western and central equatorial Africa, in: Oxford Research Encyclopedia of Climate Science.

Dezfuli, A.K., Nicholson, S.E., 2013. The Relationship of Rainfall Variability in Western Equatorial Africa to the Tropical Oceans and Atmospheric Circulation. Part II: The Boreal Autumn. J. Clim. 26, 66–84.

D.G.S., 2015. Résultats globaux du recensement général de la population et des logements de 2013 du Gabon (RGPL-2013) (Overall results of Gabon's 2013 Population and Housing Census). Direction générale de la statistique (DGS), Libreville, 247 pages..

Dieulin, C., Mahé, G., Paturel, J.-E., Ejjiyar, S., Tramblay, Y., Rouché, N., EL Mansouri, B., 2019. A New 60-Year 1940/1999 Monthly-Gridded Rainfall Data Set for Africa. Water 11, 387.

Djoufack, V., 2011. Etude multi-échelles des précipitations et du couvert végétal au Cameroun: Analyses spatiales, tendances temporelles, facteurs climatiques et anthropiques de variabilité du NDVI (Multiscale study of rainfall and vegetation cover in Cameroon : spatial analysis, temporal trends, climatic and anthropogenic factors of NDVI variability). Thesis of Université de Bourgogne.

Erazo, B., Bourrel, L., Frappart, F., Chimborazo, O., Labat, D., Dominguez-Granda, L., Matamoros, D., Mejia, R., 2018. Validation of Satellite Estimates (Tropical Rainfall

Measuring Mission, TRMM) for Rainfall Variability over the Pacific Slope and Coast of Ecuador. Water 10, 213.

Exarchou, E., Prodhomme, C., Brodeau, L., Guemas, V., Doblas-Reyes, F., 2018. Origin of the warm eastern tropical Atlantic SST bias in a climate model. Clim. Dyn. 51, 1819–1840.

Fichet, L.-V., Sannier, C., Makaga, E.M.K., Seyler, F., 2014. Assessing the accuracy of forest cover map for 1990, 2000 and 2010 at national scale in Gabon. IEEE Journal of Selected Topics in Applied Earth Observations and Remote Sensing 7, 1346–1356.

Fleischmann, A., Siqueira, V., Paris, A., Collischonn, W., Paiva, R., Pontes, P., Crétaux, J.-F., Bergé-Nguyen, M., Biancamaria, S., Gosset, M., Calmant, S., Tanimoun, B., 2018. Modelling hydrologic and hydrodynamic processes in basins with large semi-arid wetlands. J. Hydrol. 561, 943–959.

Franchito, S.H., Rao, V.B., Vasques, A.C., Santo, C.M.E., Conforte, J.C., 2009. Validation of TRMM precipitation radar monthly rainfall estimates over Brazil. J. Geophys. Res. 114, D02105.

Frappart, F., Biancamaria, S., Normandin, C., Blarel, F., Bourrel, L., Aumont, M., Azemar, P., Vu, P.-L., Le Toan, T., Lubac, B., Darrozes, J., 2018. Influence of recent climatic events on the surface water storage of the Tonle Sap Lake. Sci. Total Environ. 636, 1520–1533.

Frappart, F., Papa, F., Marieu, V., Malbeteau, Y., Jordy, F., Calmant, S., Durand, F., Bala, S., 2015. Preliminary Assessment of SARAL/AltiKa Observations over the Ganges-Brahmaputra and Irrawaddy Rivers. Mar. Geod. 38, 568–580.

Frappart, F., Ramillien, G., 2013. Changes in terrestrial water storage versus rainfall and discharges in the Amazon basin. International Journal of Climatology 33, 3029-3046. **https://doi.org/10.1002/joc.3647**

Gambotti, C., 2014. Gabon, pays émergent (Gabon, an emerging country). Geoeconomie n° 68, 159–170.

Gizaw, M.S., Gan, T.Y., 2017. Impact of climate change and El Niño episodes on droughts in sub-Saharan Africa. Clim. Dyn. 49, 665–682.

Grinsted, A., Moore, J.C., Jevrejeva, S., 2004. Application of the cross wavelet transform and wavelet coherence to geophysical time series. Nonlinear Process. Geophys. 11, 561–566.

Grist, J.P., Nicholson, S.E., 2001. A study of the dynamic factors influencing the rainfall variability in the West African Sahel. J. Clim. 14, 1337–1359.

Haug, G.H., Hughen, K.A., Sigman, D.M., Peterson, L.C., Röhl, U., 2001. Southward migration of the intertropical convergence zone through the Holocene. Science 293, 1304–1308.

Hisard, P., 1990. Variabilité des précipitations dans l'Atlantique tropical sud-est pendant un El Niño (Precipitation variability in the tropical southeast Atlantic during an El Niño). Hydrologie Continentale, Paris 5, 87–104.

Hua, W., Zhou, L., Chen, H., Nicholson, S.E., Raghavendra, A., Jiang, Y., 2016. Possible causes of the Central Equatorial African long-term drought. Environ. Res. Lett. 11, 124002.

Huffman, G.J., Adler, R.F., Arkin, P., Chang, A., Ferraro, R., Gruber, A., Janowiak, J., McNab, A., Rudolf, B., Schneider, U., 1997. The Global Precipitation Climatology Project (GPCP) Combined Precipitation Dataset. Bull. Am. Meteorol. Soc. 78, 5–20.

Jarvis, A., Reuter, H.I., Nelson, A., Guevara, E., 2008. Hole-filled SRTM for the globe Version 4, available from the CGIAR-CSI SRTM 90 m Database, available at: O (http://srtm.csi.cgiar.org).

Juárez, R.I.N., Negrón Juárez, R.I., Li, W., Fu, R., Fernandes, K., de Oliveira Cardoso, A., 2009. Comparison of Precipitation Datasets over the Tropical South American and African Continents. Journal of Hydrometeorology 10, 289-299. https://doi.org/10.1175/2008jhm1023.1

Juston, J., Seibert, J., Johansson, P.-O., 2009. Temporal sampling strategies and uncertainty in calibrating a conceptual hydrological model for a small boreal catchment. Hydrol. Process.

23, 3093–3109.

Kittel, C.M.M., Nielsen, K., Tøttrup, C., Bauer-Gottwein, P., 2018. Informing a hydrological model of the Ogooué with multi-mission remote sensing data. Hydrol. Earth Syst. Sci. 22, 1453–1472.

Kodja, D.J., 2018. Indicateurs des évènements hydroclimatiques extrêmes dans le bassin versant de l'Ouémé à l'exutoire de Bonou en Afrique de l'Ouest (Indicators of extreme hydroclimatic events in the Ouémé watershed at Bonou's outlet in West Africa). Thesis of Université Montpellier.

Kumar, P., Foufoula-Georgiou, E., 1997. Wavelet analysis for geophysical applications. Rev. Geophys. 35, 385–412.

Labat, D., Ababou, R., Mangin, A., 2000. Rainfall–runoff relations for karstic springs. Part II: continuous wavelet and discrete orthogonal multiresolution analyses. J. Hydrol. 238, 149–178.

Lienou, G., Mahe, G., Paturel, J.E., Servat, E., Sighomnou, D., Ekodeck, G.E., Dezetter, A., Dieulin, C., 2008. Evolution des régimes hydrologiques en région équatoriale camerounaise: un impact de la variabilité climatique en Afrique équatoriale? (Evolution of hydrological regimes in the equatorial area of Cameroon: an impact of climate variability in equatorial Africa?) Hydrol. Sci. J. 53, 789–801.

Lübbecke, J.F., Böning, C.W., Keenlyside, N.S., Xie, S.-P., 2010. On the connection between Benguela and equatorial Atlantic Niños and the role of the South Atlantic Anticyclone. J. Geophys. Res., Earth's Climate: The Ocean-Atmosphere Interaction 115, C09015.

Lutz, K., Jacobeit, J., Rathmann, J., 2015. Atlantic warm and cold water events and impact on African west coast precipitation. Int. J. Climatol. 35, 128–141.

Lutz, K., Rathmann, J., Jacobeit, J., 2013. Classification of warm and cold water events in the eastern tropical Atlantic Ocean. Atmos. Sci. Lett. 14, 102–106.

Mahé, G., Citeau, J., 1993. Interactions between the ocean, atmosphere and continent in Africa, related to the Atlantic monsoon flow: General pattern and the 1984 case study. Vieille de Climatologie Satellitaire 44, 34–54.

Mahé, G., Lerique, J., Olivry, J.-C., 1990. Le fleuve Ogooué au Gabon : reconstitution des débits manquants et mise en évidence de variations climatiques à l'équateur (The Ogooué River in Gabon: reconstitution of missing river discharges and evidence of climatic variations at the equator). Hydrologie Continentale 5, 105-124.

Maloba Makanga, J.D., 2015. Variabilité pluviométrique de la petite saison sèche au Gabon (Rainfall variability in the small dry season in Gabon), in: XXVIIIe Colloque de l'Association Internationale de Climatologie, Liège 2015. Université de Liège, Belgique, pp. 555-560.

Mantas, V.M., Liu, Z., Caro, C., Pereira, A.J.S.C., 2015. Validation of TRMM multi-satellite precipitation analysis (TMPA) products in the Peruvian Andes. Atmos. Res. 163, 132–145.

Maraun, D., Kurths, J., 2004. Cross wavelet analysis: significance testing and pitfalls. Nonlinear Process. Geophys. 11, 505–514.

Masson, V., Champeaux, J.-L., Chauvin, F., Meriguet, C., Lacaze, R., 2003. A Global Database of Land Surface Parameters at 1-km Resolution in Meteorological and Climate Models. J. Clim. 16, 1261–1282.

Maswood, M., Hossain, F., 2016. Advancing river modelling in ungauged basins using satellite remote sensing: the case of the Ganges–Brahmaputra–Meghna basin. International Journal of River Basin Management 14, 103–117.

McGregor, G., 2017. Hydroclimatology, modes of climatic variability and stream flow, lake and groundwater level variability: A progress report. Progress in Physical Geography: Earth and Environment 41, 496–512.

Mignard, S.L.-A., Mulder, T., Martinez, P., Charlier, K., Rossignol, L., Garlan, T., 2017. Deep-sea

terrigenous organic carbon transfer and accumulation: Impact of sea-level variations and sedimentation processes off the Ogooue River (Gabon). Mar. Pet. Geol. 85, 35–53.

New, M., Lister, D., Hulme, M., Makin, I., 2002. A high-resolution data set of surface climate over global land areas. Clim. Res. 21, 1–25.

Nicholson, S.E., 2018. The ITCZ and the Seasonal Cycle over Equatorial Africa. Bull. Am. Meteorol. Soc. 99, 337–348.

Nicholson, S.E., 1986. The Spatial Coherence of African Rainfall Anomalies: Interhemispheric Teleconnections. J. Climate Appl. Meteor. 25, 1365–1381.

Nicholson, S.E., Dezfuli, A.K., 2013. The Relationship of Rainfall Variability in Western Equatorial Africa to the Tropical Oceans and Atmospheric Circulation. Part I: The Boreal Spring. J. Clim. 26, 45–65.

Nicholson, S.E., Entekhabi, D., 1987. Rainfall Variability in Equatorial and Southern Africa: Relationships with Sea Surface Temperatures along the Southwestern Coast of Africa. J. Climate Appl. Meteor. 26, 561–578.

Nicholson, S.E., Funk, C., Fink, A.H., 2018. Rainfall over the African continent from the 19th through the 21st century. Glob. Planet. Change 165, 114–127.

Nnamchi, H.C., Li, J., Kucharski, F., Kang, I.-S., Keenlyside, N.S., Chang, P., Farneti, R., 2015. Thermodynamic controls of the Atlantic Niño. Nat. Commun. 6, 8895.

Normandin, C., Frappart, F., Diepkilé, A.T., Marieu, V., Mougin, E., Blarel, F., Lubac, B., Braquet, N., Ba, A., 2018. Evolution of the Performances of Radar Altimetry Missions from ERS-2 to Sentinel-3A over the Inner Niger Delta. Remote Sensing 10, 833.

Okumura, Y., Xie, S.-P., 2006. Some Overlooked Features of Tropical Atlantic Climate Leading to a New Niño-Like Phenomenon. J. Clim. 19, 5859–5874.

Papa, F., Bala, S.K., Pandey, R.K., Durand, F., Gopalakrishna, V.V., Rahman, A., Rossow, W.B., 2012. Ganga-Brahmaputra river discharge from Jason-2 radar altimetry: An update to the

long-term satellite-derived estimates of continental freshwater forcing flux into the Bay of Bengal. Journal of Geophysical Research: Oceans 117, C1102. https://doi.org/10.1029/2012jc008158

Paris, A., de Paiva, R.D., da Silva, J.S., Moreira, D.M., Calmant, S., Garambois, P.-A., Collischonn, W., Bonnet, M.-P., Seyler, F., 2016. Stage-discharge rating curves based on satellite altimetry and modeled discharge in the Amazon basin. Water Resources Research 52, 3787-3814. https://doi.org/10.1002/2014wr016618

Perrin, C., Oudin, L., Andreassian, V., Rojas-Serna, C., Michel, C., Mathevet, T., 2007. Impact of limited streamflow data on the efficiency and the parameters of rainfall—runoff models. Hydrol. Sci. J. 52, 131–151.

Pontes, P.R.M., Fan, F.M., Fleischmann, A.S., de Paiva, R.C.D., Buarque, D.C., Siqueira, V.A., Jardim, P.F., Sorribas, M.V., Collischonn, W., 2017. MGB-IPH model for hydrological and hydraulic simulation of large floodplain river systems coupled with open source GIS. Environmental Modelling & Software 94, 1–20.

Pozo-Vázquez, D., Esteban-Parra, M.J., Rodrigo, F.S., Castro-Díez, Y., 2001. A study of NAO variability and its possible non-linear influences on European surface temperature. Clim. Dyn. 17, 701–715.

Ramillien, G., Frappart, F., Güntner, A., Ngo-Duc, T., Cazenave, A., Laval, K., 2006. Time variations of the regional evapotranspiration rate from Gravity Recovery and Climate Experiment (GRACE) satellite gravimetry. Water Resour. Res. 42, W10403.

Razavi, S., Tolson, B.A., 2013. An efficient framework for hydrologic model calibration on long data periods. Water Resour. Res. 49, 8418–8431.

Saf, O., 2018. L3C hourly Sea Surface Temperature (GHRSST) data record release 1 – MSG, EUMETSAT SAF on Ocean and Sea Ice. https://doi.org/10.15770/EUM_SAF_OSI_0004

Sannier, C., McRoberts, R.E., Fichet, L.-V., Makaga, E.M.K., 2014. Using the regression

estimator with Landsat data to estimate proportion forest cover and net proportion deforestation in Gabon. Remote Sens. Environ. 151, 138–148.

Santoso, A., Mcphaden, M.J., Cai, W., 2017. The Defining Characteristics of ENSO Extremes and the Strong 2015/2016 El Niño. Rev. Geophys., AMS 87th Annual Meeting 55, 1079–1129.

Scheel, M.L.M., Rohrer, M., Huggel, C., Santos Villar, D., Silvestre, E., Huffman, G.J., 2011. Evaluation of TRMM Multi-satellite Precipitation Analysis (TMPA) performance in the Central Andes region and its dependency on spatial and temporal resolution. Hydrol. Earth Syst. Sci. 15, 2649–2663.

Shannon, L.V., Boyd, A.J., Brundrit, G.B., Taunton-Clark, J., 1986. On the existence of an El Niño-type phenomenon in the Benguela system. J. Mar. Res. 44, 495–520.

Singhrattna, N., Rajagopalan, B., Krishna Kumar, K., Clark, M., 2005. Interannual and Interdecadal Variability of Thailand Summer Monsoon Season. Journal of Climate 18, 1697-1708. https://doi.org/10.1175/jcli3364.1

Siqueira, V.A., Fleischmann, A., Jardim, P.F., Fan, F.M., Collischonn, W., 2016. IPH-Hydro Tools: a GIS coupled tool for watershed topology acquisition in an open-source environment. RBRH 21, 274–287.

Siqueira, V.A., Paiva, R.C.D., Fleischmann, A.S., Fan, F.M., Ruhoff, A.L., Pontes, P.R.M., Paris, A., Calmant, S., Collischonn, W., 2018. Toward continental hydrologic-hydrodynamic modeling in South America. Hydrol. Earth Syst. Sci. 22, 4815–4842.

Sood, A., Smakhtin, V., 2015. Global hydrological models: a review. Hydrol. Sci. J. 60, 549–565.

Sutton, R.T., Dong, B., Gregory, J.M., 2007. Land/sea warming ratio in response to climate change: IPCC AR4 model results and comparison with observations. Geophys. Res. Lett. 34, L02701.

Tierney, J.E., Russell, J.M., Huang, Y., Damsté, J.S.S., Hopmans, E.C., Cohen, A.S., 2008. Northern hemisphere controls on tropical southeast African climate during the past 60,000

years. Science 322, 252–255.

Todd, M.C., Washington, R., 2004. Climate variability in central equatorial Africa: Influence from the Atlantic sector. Geophys. Res. Lett. 31, L23202. https://doi.org/10.1029/2004GL020975

Tomkins, K.M., 2014. Uncertainty in streamflow rating curves: methods, controls and consequences. Hydrol. Process. 28, 464–481.

Torrence, C., Compo, G.P., 1998. A Practical Guide to Wavelet Analysis. Bull. Am. Meteorol. Soc. 79, 61–78.

Torrence, C., Webster, P.J., 1999. Interdecadal Changes in the ENSO–Monsoon System. J. Clim. 12, 2679–2690.

van den Dool, H.M., Saha, S., Johansson, Å., 2000. Empirical Orthogonal Teleconnections. J. Clim. 13, 1421–1435.

Vu, P.L., Ha, M.C., Frappart, F., Darrozes, J., Ramillien, G., 2019. Identifying 2010 Xynthia Storm Signature in GNSS-R-Based Tide Records. Remote Sensing 11, 782.

Witman, S., 2017. River Plumes near the Equator Have Major Effects on Oceans. EOS, 98. https://doi.org/10.1029/2017EO073461

Wu, G., Liu, Y., He, B., Bao, Q., Duan, A., Jin, F.-F., 2012. Thermal Controls on the Asian Summer Monsoon. Scientific Reports 2, 404. https://doi.org/10.1038/srep00404

Yun, K.-S., Yeh, S.-W., Ha, K.-J., 2019. Underlying mechanisms leading to El Niño-to-La Niña transition are unchanged under global warming. Clim. Dyn. 52, 1723–1738.

Zebiak, S.E., 1993. Air–Sea Interaction in the Equatorial Atlantic Region. J. Clim. 6, 1567–1586.

Zulkafli, Z., Buytaert, W., Onof, C., Manz, B., Tarnavsky, E., Lavado, W., Guyot, J.-L., 2014. A Comparative Performance Analysis of TRMM 3B42 (TMPA) Versions 6 and 7 for Hydrological Applications over Andean–Amazon River Basins. J. Hydrometeorol. 15, 581–592.

Figures

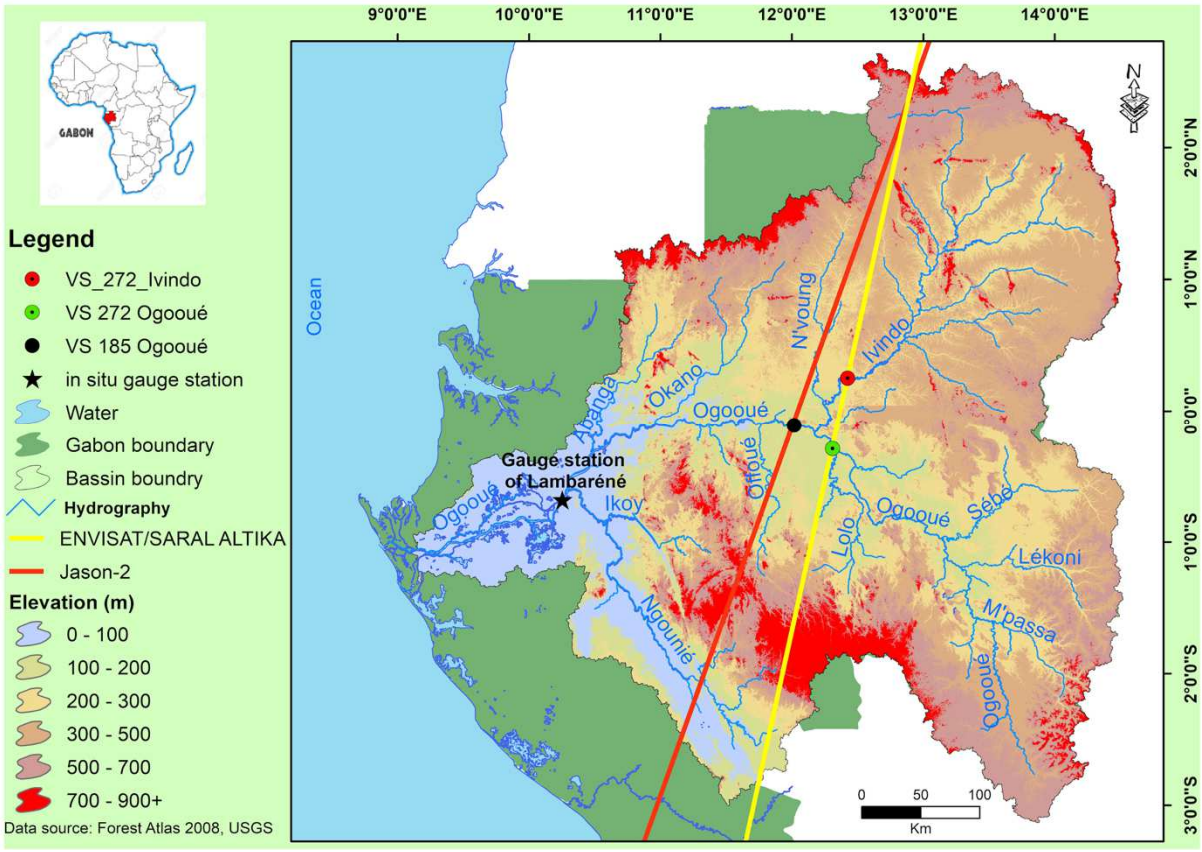

Figure 1: Hydrography of the ORB (Gabon) based on the Forest Atlas (USGS, 2008). The in situ gauge station of Lambaréné and the altimetry VS are represented using black star and dots (green, red and black) respectively.

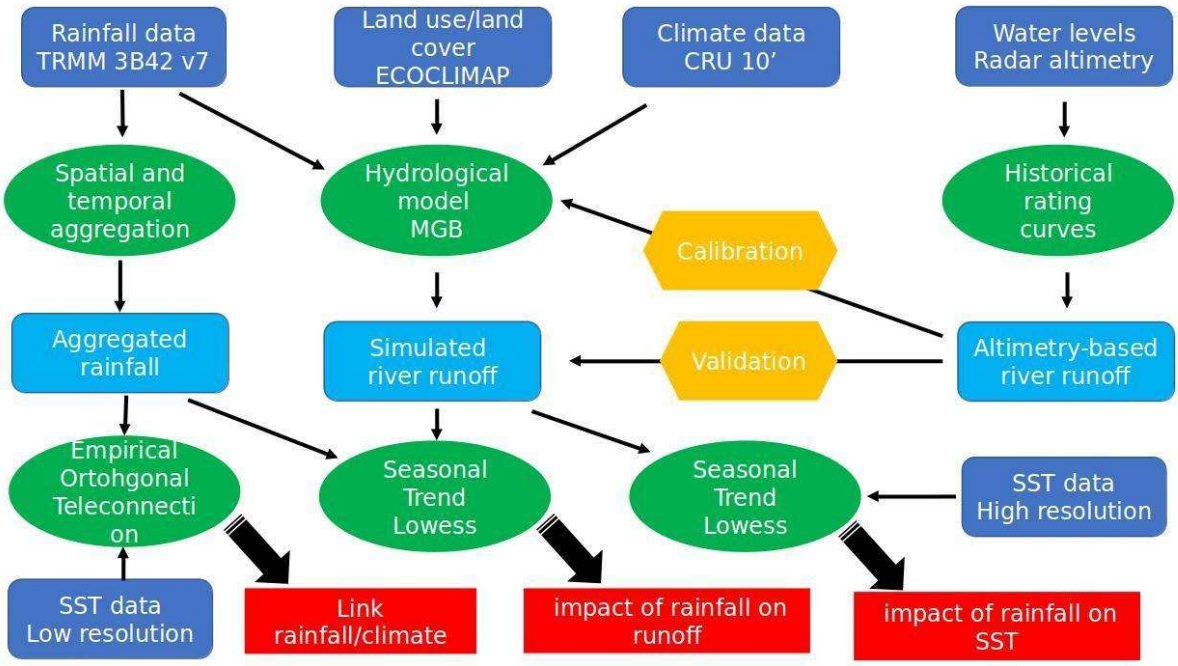

Figure 2: work-flow summarizing the whole methodology used

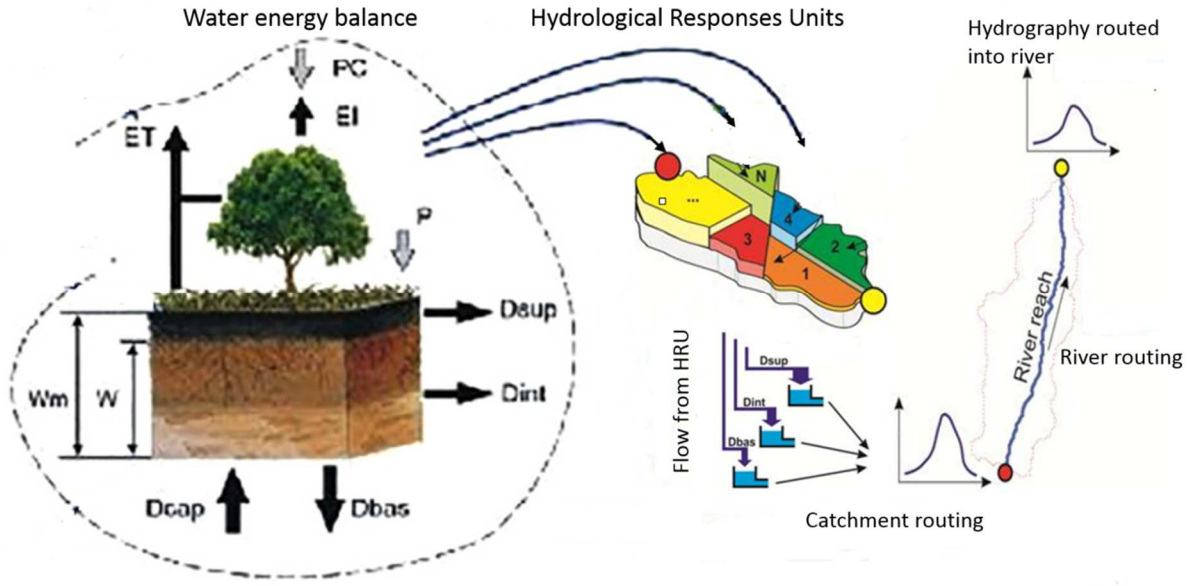

Figure 3: Main processes represented in the MGB model, including PC: precipitation; ET: evapotranspiration; EI: evaporation of intercepted water; P: precipitation discounted by EI; Dsup: surface flow; Dint: subsurface flow; Dbas: groundwater flow; Dcap: capillary flux; W: soil water storage; Wm: maximum soil water storage; E: open water evaporation (source: Siquiera et al. (2018)).

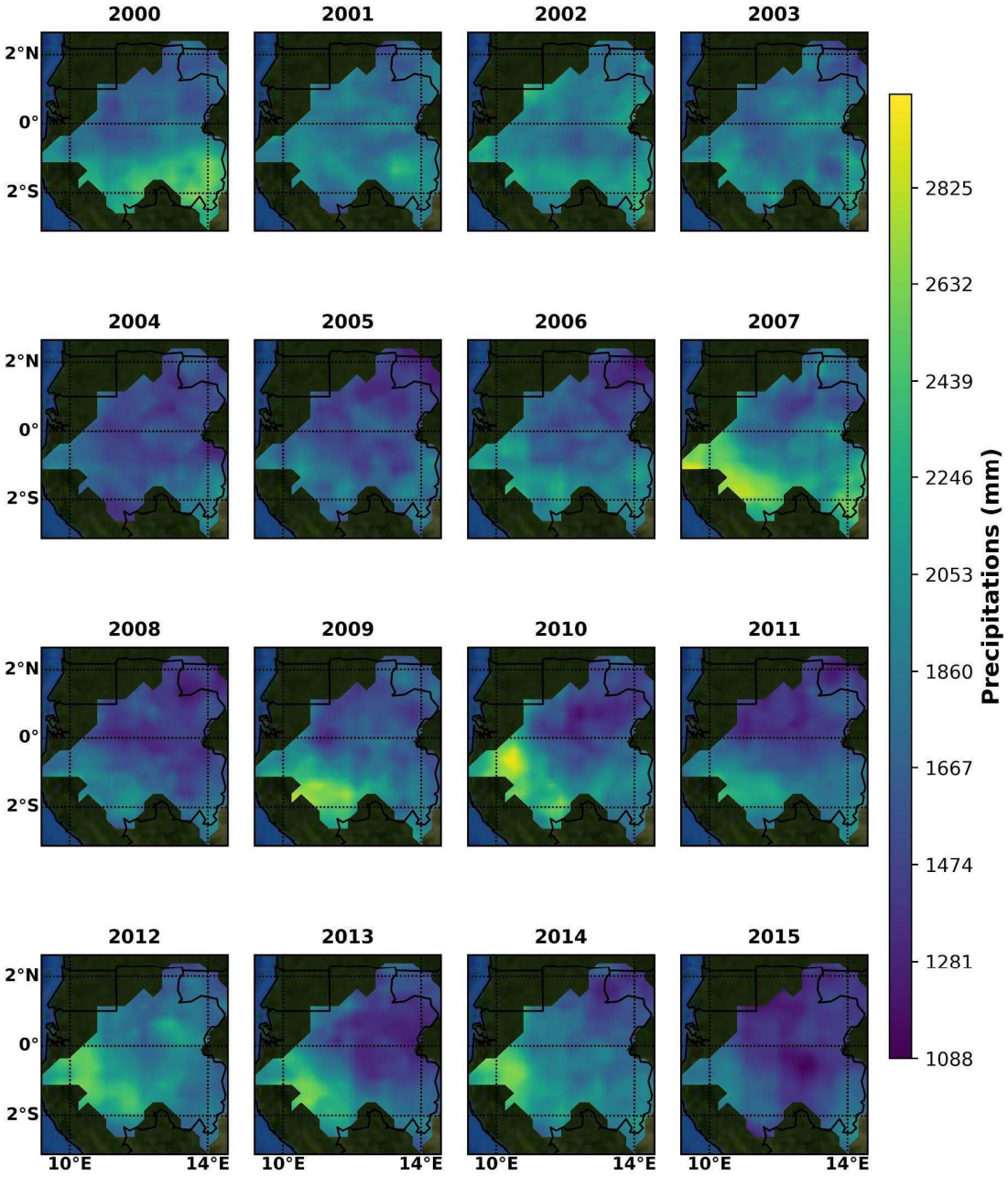

Figure 4: Annual distribution of rainfall in the ORB.

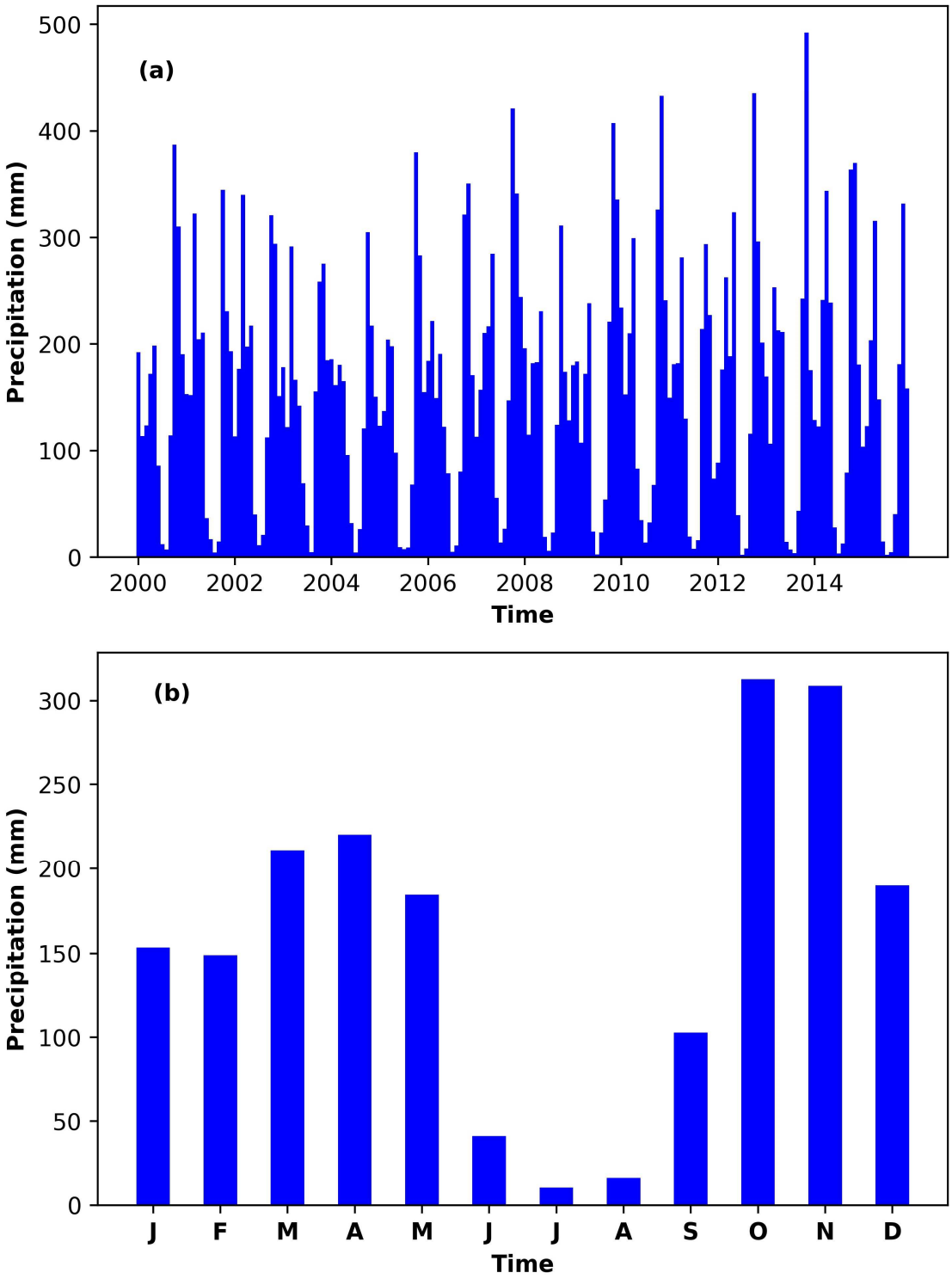

Figure 5: Monthly (a) and monthly average (b) rainfall in the ORB from 2000 to 2015.

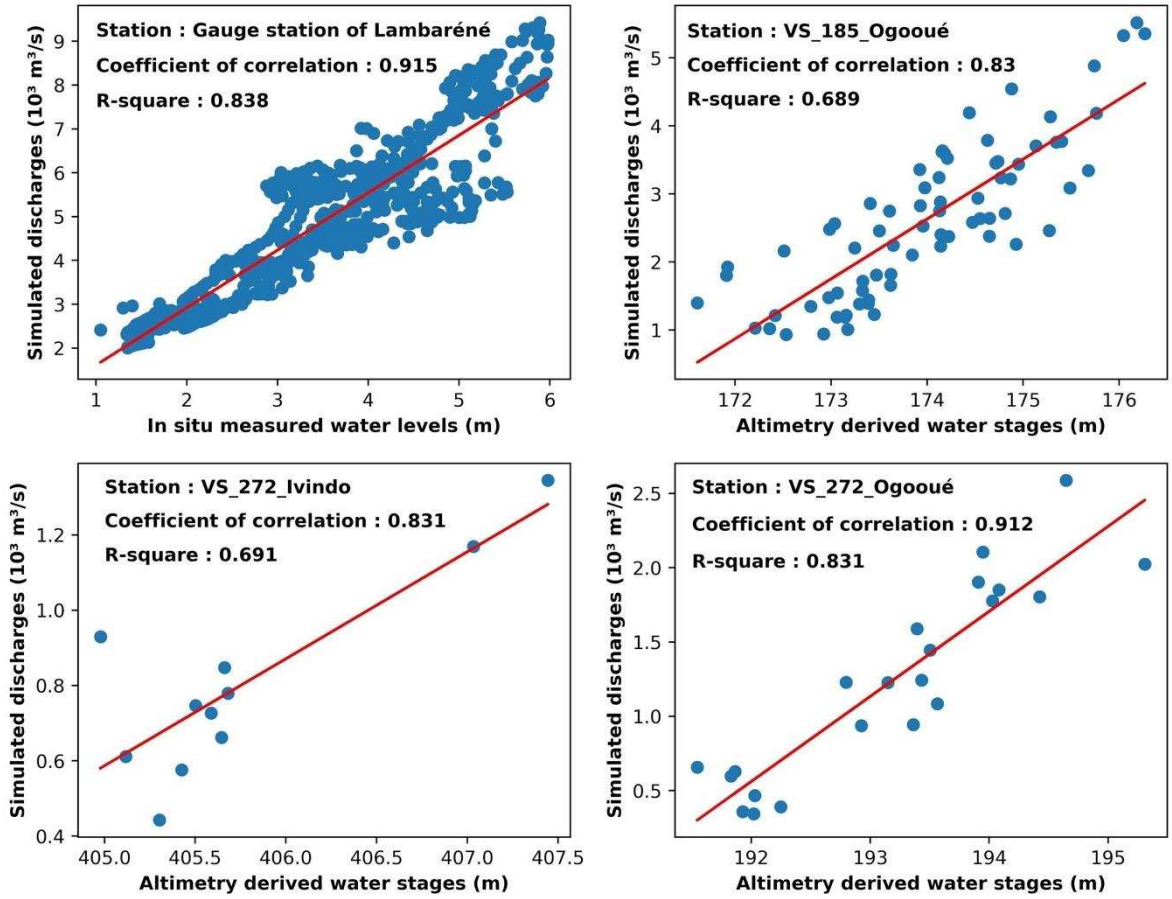

Figure 6: Scatterplots of water stages and simulated discharges at calibrated stations of the ORB.

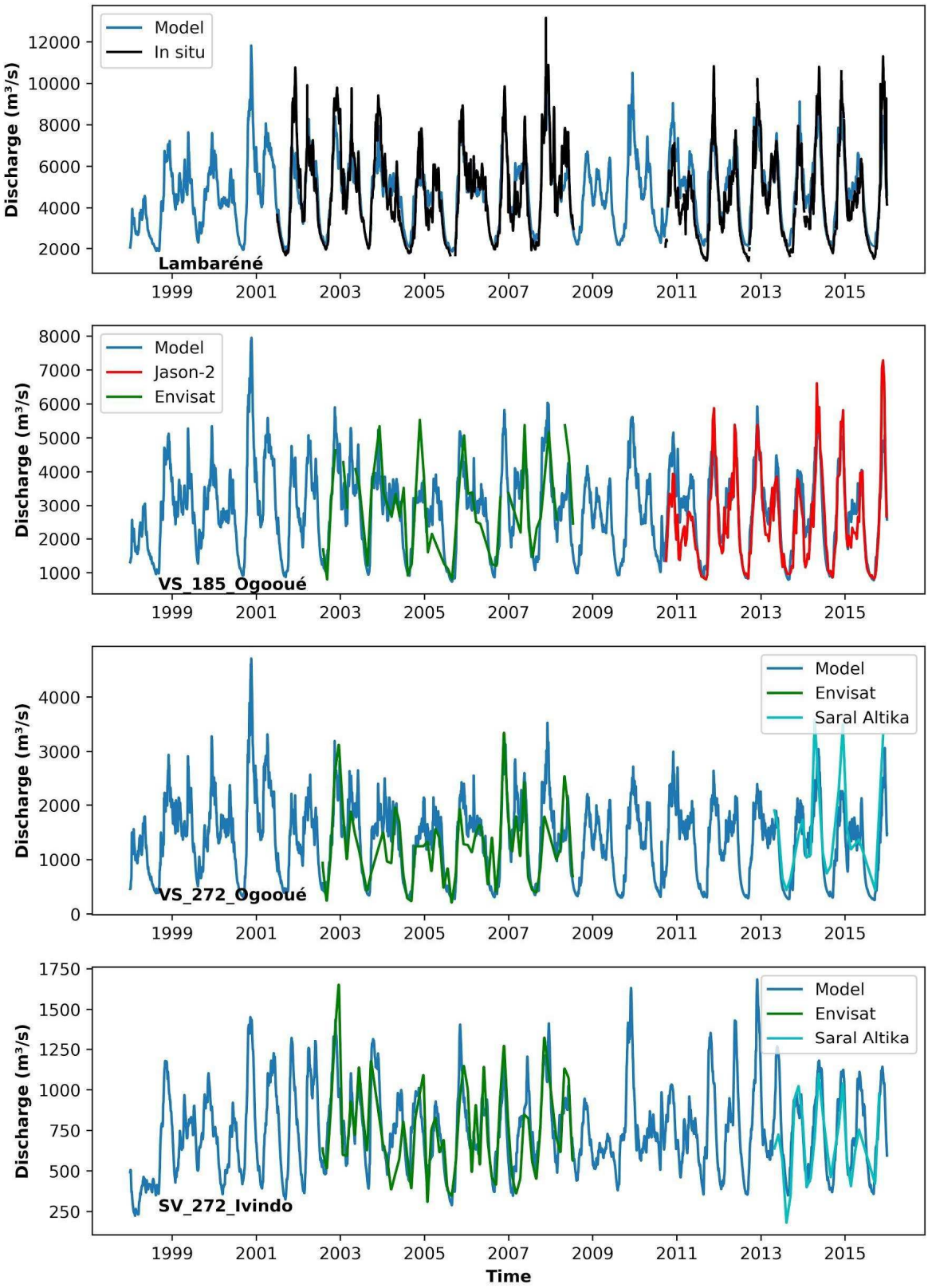

Figure 7: validation of simulated discharges with in situ measured and altimetry derived discharges

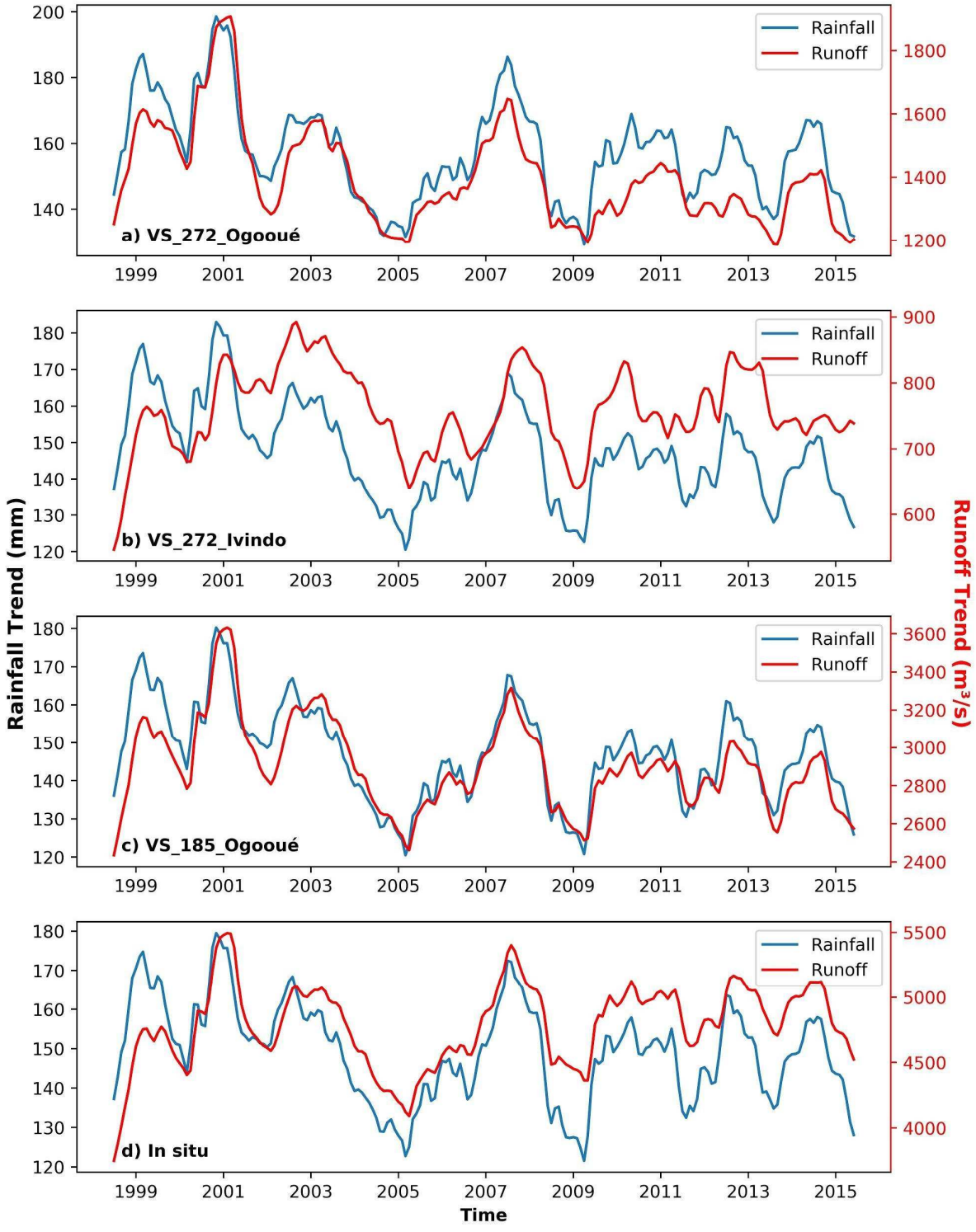

Figure 8: STL decomposition components of rainfall (blue) and river discharge (red) trend components for the four drainage areas of this study.

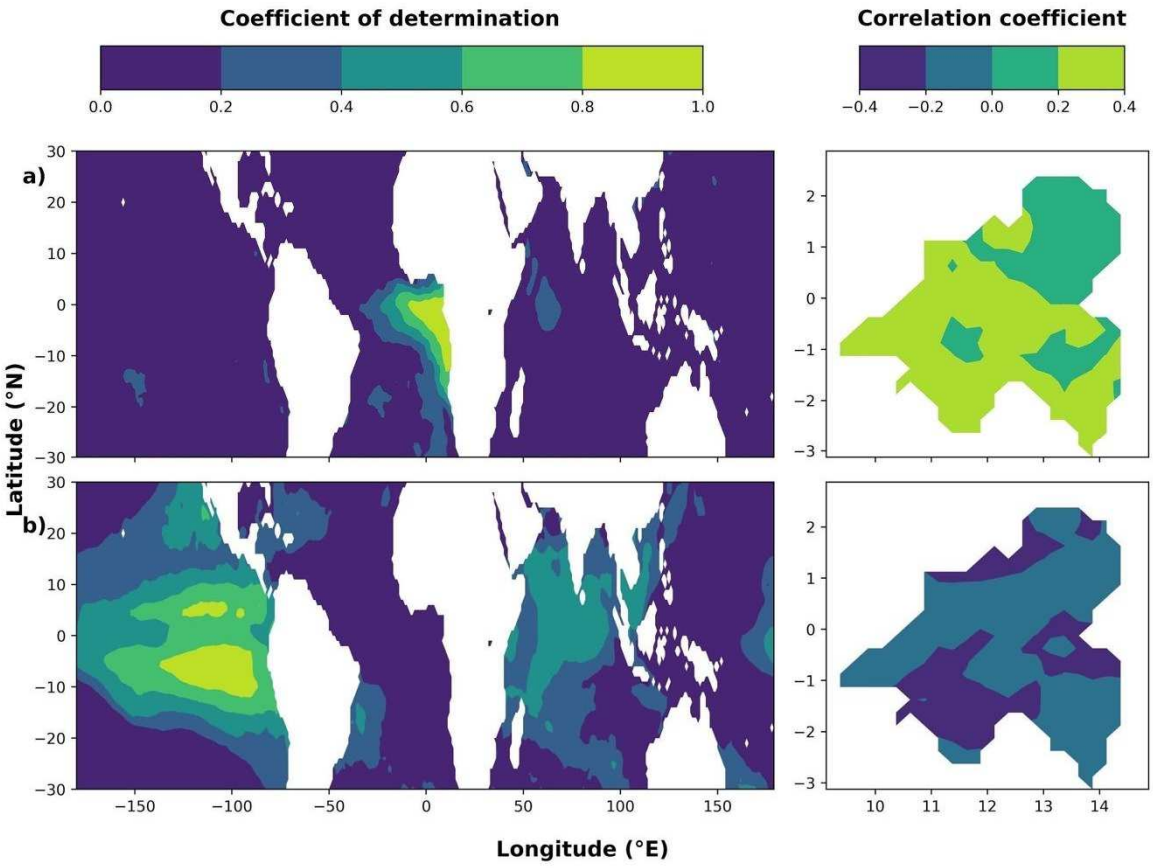

Figure 9: The two first modes of EOT analysis applied in 1998 - 2015 precipitations and 1° X 1° global tropical SSTs: a) is the first mode and b) is the second mode.

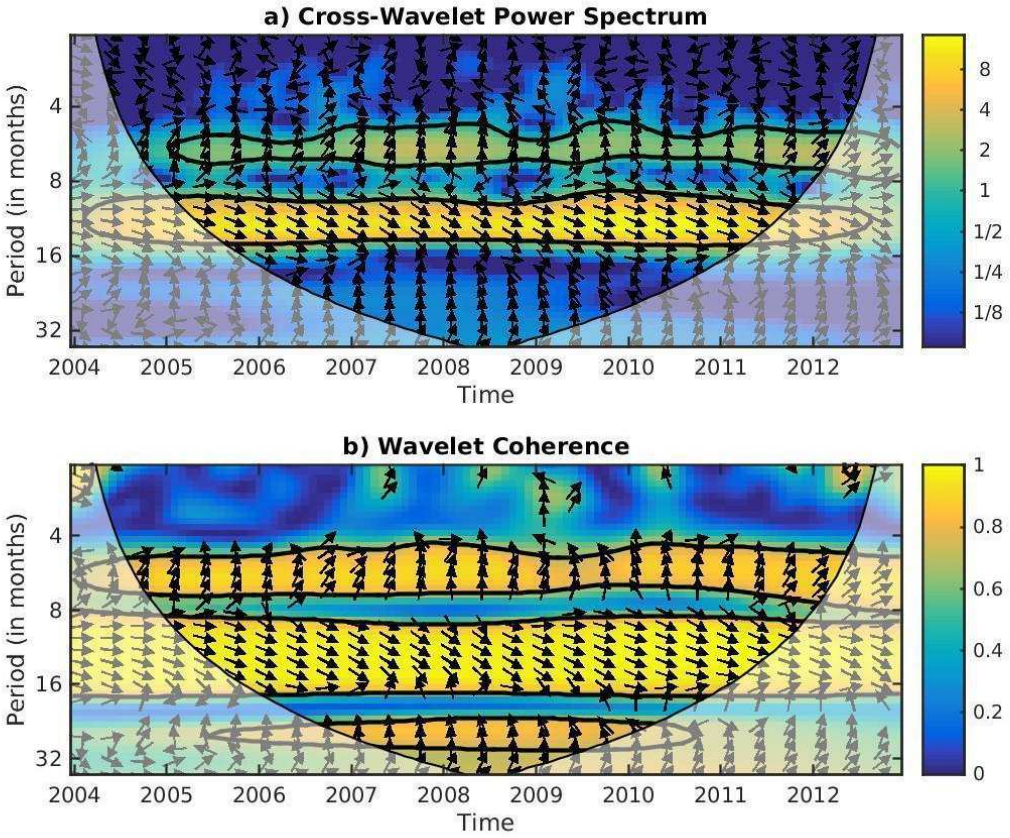

Figure 10: Cross-wavelet transform between the spatially average time series of SST in the mouth of the Ogooué River and the Ogooué River discharge time series. Arrows indicate the phase of coherence: right = in-phase, left = anti-phase and intermediate direction denote angular leading of one time series by another. Black solid lines delineate time-frequency areas of significant cross wavelet coherence between both time series.

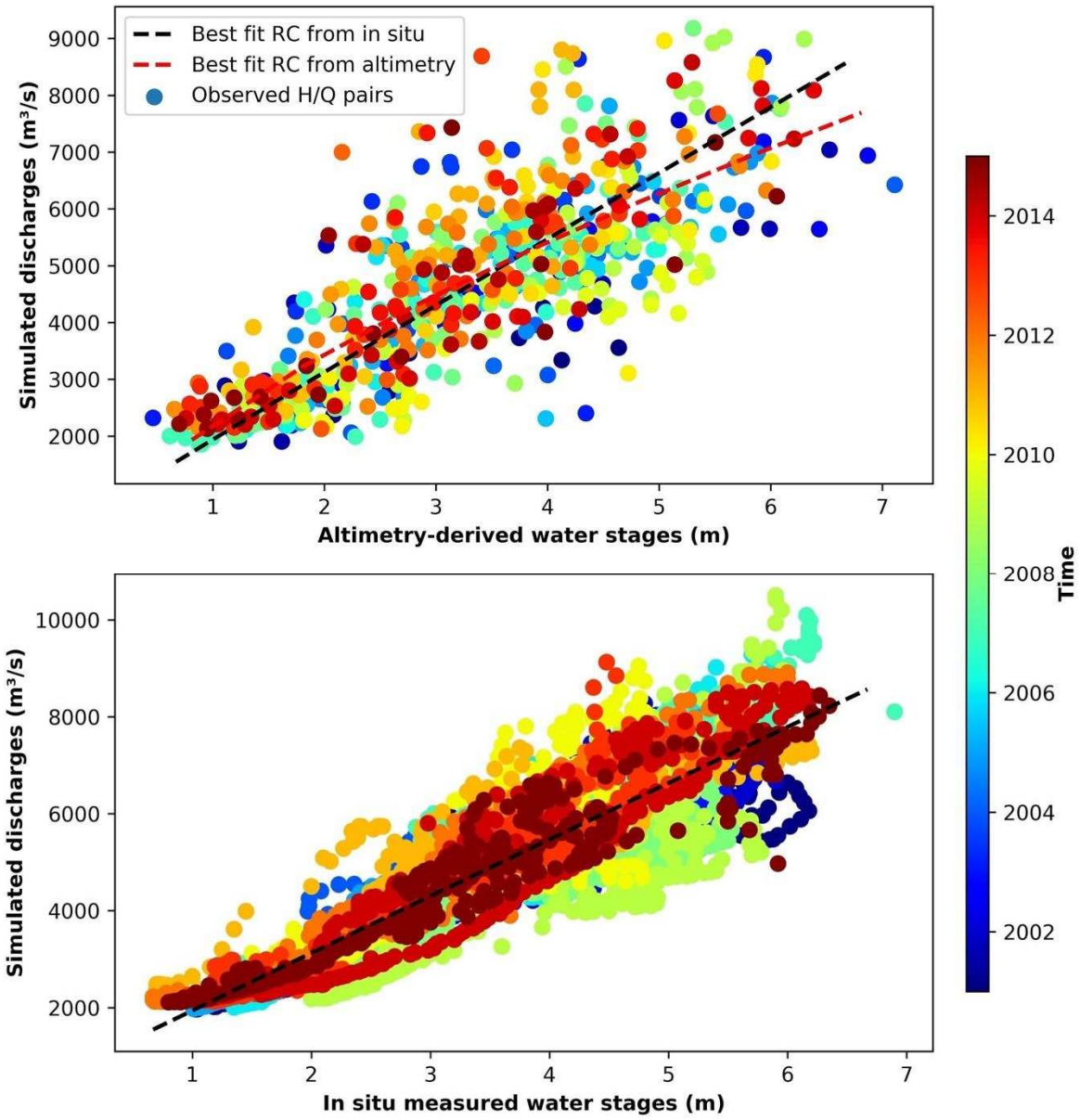

Figure 11: rating curves in Lambaréné from in situ and altimetry derived water surface stages and modeled river discharges .

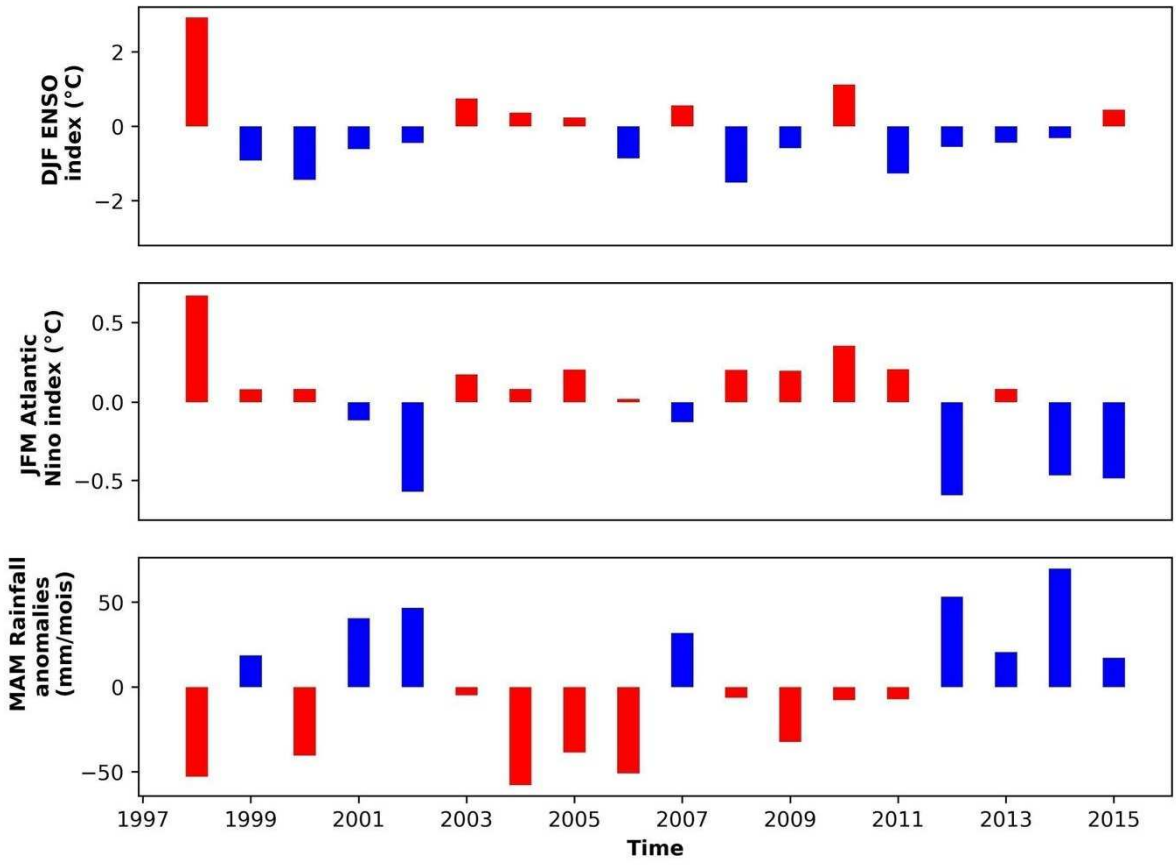

Figure 12: interannual variations of: (i) ENSO 3.4 average over December-February, (ii) tropical Atlantic Niño indice average over January-March and (iii) rainfall anomalies averaged over March-May.

Tables

Table 1: Main characteristics of VSs (Bogning et al. 2018) used in this study

Virtual Stations	Missions	Longitude	Latitude	Mean river width (Km)
VS_272_Ivindo	Envisat, Saral Altika	12.4228	0.2542	0.20
VS_272_Ogooué	Envisat, Saral Altika	12.3051	-0.2816	0.36
VS_315_Ogooué	Envisat	11.6422	−0.0618	0.37
VS_185_Ogooué	Jason-2	12.0035	0.1148	0.36

Table 2: Statistical results of the MGB calibration in the ORB

Stations	Longitude (°E)	Latitude (°N)	Drainage area (km²)	Source of data	calibration period	NSE	NSElog	ΔV (%)
VS_272_Ivindo	12.8135	0.5371	49115	Envisat	2008 - 2010	0.70	0.51	2.96
VS_272_Ogooue	12.6932	-0.8254	46143	Envisat	2008 - 2010	0.80	0.82	-5.67
VS_185_Ogooué	11.9393	-0.1083	130844	Jason 2	2008 - 2010	0.66	0.61	-11.91
Lambaréné gauge station	10.3634	-0.5867	205082.57	In situ	2008 - 2010	0.76	0.81	0.70

Table 3 : Cross-correlations of rainfall and river discharges time series

	Original time series		Trend components of time series	
	Correlation coefficient	lags	Correlation coefficient	lags
VS_272_Ivindo	0.73	1	0.56	0
VS_272_Ogooué	0.88	1	0.88	0
VS_185_Ogooué	0.89	1	0.82	0
Lambaréné Ggauge station	0.90	1	0.87	0